

1   **A mutation-independent approach via transcriptional upregulation of a disease  
2   modifier gene rescues muscular dystrophy *in vivo***

3

4   Dwi U. Kemaladewi<sup>1,\*</sup>, Prabhpreet S. Bassi<sup>1,2,\*</sup>, Steven Erwood<sup>1,2</sup>, Dhekra Al-Basha<sup>3,4</sup>,  
5   Kinga I. Gawlik<sup>5</sup>, Kyle Lindsay<sup>1</sup>, Ella Hyatt<sup>1</sup>, Rebekah Kember<sup>1</sup>, Kara M. Place<sup>1</sup>, Ryan M.  
6   Marks<sup>1</sup>, Madeleine Durbejj<sup>5</sup>, Steven A. Prescott<sup>3,4,6</sup>, Evgueni A. Ivakine<sup>1,\*\*</sup>, Ronald D.  
7   Cohn<sup>1,2,7,\*\*</sup>

8

9   <sup>1</sup>Program in Genetics and Genome Biology, the Hospital for Sick Children Research  
10 Institute, Toronto, Canada

11   <sup>2</sup>Department of Molecular Genetics, University of Toronto, Canada

12   <sup>3</sup>Program in Neuroscience and Mental Health, the Hospital for Sick Children Research  
13 Institute, Toronto, Canada

14   <sup>4</sup>Department of Physiology, University of Toronto, Canada

15   <sup>5</sup>Unit of Muscle Biology, Department of Experimental Medical Science, Lund University,  
16 Lund, Sweden

17   <sup>6</sup>Institute of Biomaterials and Biomedical Engineering, University of Toronto, Canada

18   <sup>7</sup>Department of Pediatrics, the Hospital for Sick Children, Toronto, Canada

19   \*These authors contributed equally to this work

20   \*\*These authors contributed equally to this work

21

22

23

24 **Introductory paragraph**

25 Identification of genetic modifiers has provided critically important insights into the  
26 pathogenesis and heterogeneity of disease phenotypes in individuals affected by  
27 neuromuscular disorders (NMDs). Targeting modifier genes to improve disease  
28 phenotypes could be especially beneficial in cases where the causative genes are large,  
29 structurally complex and the mutations are heterogeneous. Here, we report a mutation-  
30 independent strategy to upregulate expression of a compensatory disease-modifying  
31 gene in Congenital Muscular Dystrophy type 1A (MDC1A) using a CRISPR/dCas9-  
32 based transcriptional activation system.

33 MDC1A is caused by nonfunctional Laminin  $\alpha$ 2, which compromises muscle fibers  
34 stability and axon myelination in peripheral nerves <sup>1</sup>. Transgenic overexpression of  
35 *Lama1*, encoding a structurally similar protein Laminin  $\alpha$ 1, ameliorates muscle wasting  
36 and paralysis in the MDC1A mouse models, demonstrating its important role as a  
37 disease modifier <sup>2</sup>. Yet, upregulation of *Lama1* as a postnatal gene therapy is hampered  
38 by its large size, which exceeds the current genome packaging capacity of clinically  
39 relevant delivery vehicles such as adeno-associated viral vectors (AAVs).

40 In this study, we use the CRISPR/dCas9-based transcriptional activation system to  
41 upregulate *Lama1*. This system is comprised of catalytically inactive *S. aureus* Cas9  
42 (dCas9) fused to VP64 transactivation domains and sgRNAs targeting the *Lama1*  
43 promoter. We first demonstrate robust upregulation of *Lama1* in myoblasts, and  
44 following AAV9-mediated intramuscular delivery, in skeletal muscles of  $dy^{2j}/dy^{2j}$  mouse  
45 model of MDC1A.

46 We therefore assessed whether systemic upregulation of *Lama1* would yield therapeutic  
47 benefits in  $dy^{2j}/dy^{2j}$  mice. When the intervention was started early in pre-symptomatic  
48  $dy^{2j}/dy^{2j}$  mice, *Lama1* upregulation prevented muscle fibrosis and hindlimb paralysis. An  
49 important question for future therapeutic approaches for a variety of disorders relates to  
50 the therapeutic window and phenotypic reversibility. This is particularly true for muscular  
51 dystrophies as it has long been hypothesized that fibrotic changes in skeletal muscle  
52 represent an irreversible disease state that would impair any therapeutic intervention at  
53 advanced stages of the disease. Here, we demonstrate that dystrophic features and  
54 disease progression were significantly improved and reversed when the treatment was  
55 initiated in symptomatic 3-week old  $dy^{2j}/dy^{2j}$  mice with already-apparent hind limb  
56 paralysis and significant muscle fibrosis.

57 Collectively, our data demonstrate the feasibility and therapeutic benefit of  
58 CRISPR/dCas9-mediated modulation of a disease modifier gene, which opens up an  
59 entirely new and mutation-independent treatment approach for all MDC1A patients.  
60 Moreover, this treatment strategy provides evidence that muscle fibrosis can be  
61 reversible to some degree, thus extending the therapeutic window for this disorder. Our  
62 data provide a proof-of-concept strategy that can be applied to a variety of disease  
63 modifier genes and a powerful therapeutic approach for various inherited and acquired  
64 diseases.

65  
66

67 Congenital muscular dystrophy 1A (MDC1A) is an autosomal recessive neuromuscular  
68 disease associated with a high degree of morbidity and mortality in early childhood<sup>1</sup>. It is  
69 caused by mutations in the *LAMA2* gene encoding Laminin α2 chain (*LAMA2*), which  
70 interacts with the β1 and γ1 chains to form the heterotrimer Laminin-211, an extracellular  
71 matrix protein (reviewed in<sup>3</sup>). Laminin-211 interacts with α-dystroglycan and α7β1  
72 integrin in skeletal muscle and Schwann cells, providing the necessary roles such as  
73 survival and stability of myotubes, as well as proper neurite growth, axon myelination  
74 and migration of Schwann cells. Lack of Laminin-211 in MDC1A causes degeneration of  
75 skeletal muscle and impaired Schwann cell differentiation, resulting in a cascade of  
76 secondary events including apoptosis/necrosis of muscle fibers, inflammation, and  
77 fibrosis, which ultimately precipitate the disease. Despite significant advances in our  
78 understanding of MDC1A pathophysiology, currently, there is no cure.  
79 Due to the genetic nature of the disease, gene therapy is a promising treatment option  
80 for MDC1A. The large size of *LAMA2* transcript, however, presents a challenge with  
81 respect to gene delivery. We have recently overcome this challenge by using  
82 CRISPR/Cas9 technology to correct a mutation in *Lama2* gene *in vivo*<sup>4</sup>. We focused on  
83 *dy<sup>2j</sup>/dy<sup>2j</sup>* mouse model, which harbors a splice site mutation in *Lama2* causing  
84 spontaneous exon skipping and truncation of N-terminal domain of the protein<sup>5</sup>. We  
85 developed an exon inclusion strategy to correct the splice mutation, leading to  
86 restoration of full-length *Lama2*. This study established the first direct correction of the  
87 primary genetic defect underlying MDC1A in an *in vivo* model.  
88 To date, there are over 350 reported pathogenic nonsense-, missense-, splice site- and  
89 deletion mutations in the *LAMA2* gene. Given the variety of MDC1A-causing genomic  
90 alterations, CRISPR/Cas9-mediated gene editing strategies would require design and  
91 thorough analysis of multiple sgRNAs specific for each individual mutation. Moreover,  
92 safety concerns regarding CRISPR/Cas9's potential mutagenic nature and the presence  
93 of off-target effects after gene editing remain, which together may prove to be  
94 challenging from a safety and regulatory point-of-view. In contrast, the attenuation of  
95 disease pathogenicity by targeted modulation of disease modifier gene expression would  
96 be a potentially safer alternative and beneficial to all individuals with MDC1A.  
97 One of the strongest reported disease modifiers for MDC1A is Laminin-α1 protein, which  
98 is structurally similar to Laminin-α2 (**Fig. 1a**). However, Laminin-α1 is not expressed in  
99 skeletal muscles or Schwann cells. A series of studies previously demonstrated that  
100 transgenic expression of *Lama1*, encoding Laminin-α1, rescued both myopathy and

101 peripheral neuropathy in  $dy^{2j}/dy^{2j}$ <sup>6</sup> and  $dy^{3K}/dy^{3K}$ <sup>2,7-10</sup>, the latter also showed increased  
102 lifespan. Although these studies firmly established compensatory function of Laminin- $\alpha$ 1  
103 in MDC1A, utilization of this modifier as a postnatal gene therapy is hampered by the  
104 size of *Lama1* cDNA, which exceeds the 4.7 kb packaging capacity of AAV vectors.  
105 Advances in CRISPR/Cas9 technologies have provided opportunities for regulating gene  
106 expression and creating epigenetic alterations without introducing DNA double-strand  
107 breaks (DSBs); commonly termed CRISPR transcriptional activation/inhibition system.  
108 The strategy utilizes nuclease-deficient Cas9 (dCas9), which is unable to cleave DNA  
109 due to mutations within the nuclease domains, but still retains the ability to specifically  
110 bind to DNA when guided by a single guide RNA (sgRNA)<sup>11,12</sup>. Using the originally  
111 described *S. pyogenes* (*Sp*) dCas9 fused to multiple copies of the VP16 transcriptional  
112 activator, our group and others have demonstrated utilization of the CRISPR/dCas9  
113 system to upregulate expression of modifier genes *in vitro*<sup>11-14</sup>. A major challenge for *in*  
114 *vivo* applications lies in the large size of *SpdCas9* and its transcriptional activator fusion  
115 derivatives that exceed AAV genome packaging capacity. To accommodate this  
116 limitation, we sought to adapt the transcriptional upregulation system and utilize a  
117 significantly smaller Cas9 protein derived from *S. aureus* (*Sa*)<sup>15</sup> to upregulate MDC1A  
118 modifier *Lama1*. We hypothesized that CRISPR/dCas9-mediated transcriptional  
119 upregulation of *Lama1* would be sufficient to compensate for the lack of *Lama2* and  
120 ameliorate disease phenotypes in  $dy^{2j}/dy^{2j}$  mice.  
121 First, we mutagenized SaCas9 endonuclease catalytic residues (D10A, N580A) to  
122 create SadCas9 and then fused it to transcriptional activators VP64 (four copies of  
123 VP16) on both N- and C-termini (**Fig. S1**). We tested the ability of the system, denoted  
124 as SadCas9-2xVP64, to upregulate the expression of minCMV-driven *tdTomato* gene in  
125 293T cells<sup>16</sup>. In the absence of the SadCas9-2xVP64, the expression of *tdTomato* was  
126 undetectable due to the low baseline activity of minCMV promoter (**Fig. S1a, b**). In the  
127 presence of SadCas9-2xVP64 in combination with an sgRNA targeting the minCMV  
128 locus, we observed high *tdTomato* fluorescence signal (**Fig. S1c, d**), indicating the  
129 general applicability of this system to modulate expression of a gene of interest.  
130 Subsequently, we tailored the system to upregulate *Lama1* expression and designed five  
131 sgRNAs, denoted as g1 to g5, within the 500 nucleotides region immediately upstream  
132 of the *Lama1* transcription start site (**Figs. 1b, c**). When co-expressed with SadCas9-  
133 VP64 in C2C12 murine myoblasts, 3 out of 5 sgRNAs, namely g1, g2, and g5  
134 consistently induced significant increase of *Lama1* transcript expression (**Figs. 1d, e**).

135 Although all sgRNAs were designed to target a chromatin-accessible region derived  
136 from DNase1 hypersensitivity- and assay for transposase-accessible chromatin (ATAC-  
137 Seq) sites (**Fig. 1b**), g3 and g4 failed to increase expression of *Lama1* above the basal  
138 level. This corroborates previously reported findings that chromatin accessibility is not a  
139 reliable predictor of successful gene activation<sup>12,17,18</sup>. Nonetheless, the sgRNA closest to  
140 the transcription start site, g1, and the combination of the three most optimum sgRNAs  
141 (g1, g2, g5) resulted in a robust increase in *Lama1* protein expression in *dy<sup>2j</sup>/dy<sup>2j</sup>*-derived  
142 myoblasts (**Figs. 1f, 1g**), warranting further investigation *in vivo*.

143 We then treated 3-week-old *dy<sup>2j</sup>/dy<sup>2j</sup>* mice with an AAV9 carrying FLAG-tagged  
144 SadCas9-2xVP64 in the absence of sgRNA (no guide) or with g1 (single guide) or a  
145 combination of g1, g2 and g5 (three guides) (**Fig. 2a**). Due to the packaging capacity of  
146 the AAV, the dCas9-2xVP64 and the three guides were split into two vectors (**Fig. 2a**).  
147 Each mouse received a single intramuscular injection of  $7.5 \times 10^{11}$  viral genomes of  
148 AAV9, which was doubled to  $1.5 \times 10^{12}$  viral genomes total for the three guide cohort, in  
149 the right *tibialis anterior* (TA) and was sacrificed 4 weeks post injection. FLAG  
150 expression was detected by western blot in all SadCas9-2xVP64-injected right TA  
151 muscles, however, only those injected with guide-containing constructs showed *Lama1*  
152 upregulation (**Fig. 2b**). Similarly, immunofluorescence staining revealed sarcolemmal  
153 expression of *Lama1* (**Fig. 2c**, upper), indicating proper protein localization.  
154 Furthermore, H&E staining exhibited considerably improved muscle architecture (**Fig.**  
155 **2c**, lower) in the single- and three guide treatment groups, as compared to the no guide  
156 controls.

157 Next, we sought to investigate whether upregulation of *Lama1* could be achieved  
158 systemically *in vivo* and, if administered into pre-symptomatic neonatal *dy<sup>2j</sup>/dy<sup>2j</sup>* mice,  
159 would prevent the manifestation of dystrophic pathophysiology and paralysis. AAV9  
160 particles carrying either no guide or a combination of three guides were injected into the  
161 temporal vein of 2-day-old (P2) *dy<sup>2j</sup>/dy<sup>2j</sup>* mice (**Fig. 3a**). Seven weeks post injection, the  
162 animals that received the three guides treatment showed an absence of classical  
163 hindlimb contracture, unlike the control group (**Fig. 3b; Supplementary videos 1 and**  
164 **2**). Western blot, immunofluorescence and H&E staining of TA and gastrocnemius  
165 muscles demonstrated robust expression of *Lama1* on the sarcolemmal membrane (**Fig.**  
166 **3c, 3d**), leading to ~50% reduction of fibrosis (**Figs. 3e, 3f, S2**).

167 We subsequently examined the ability of *Lama1* upregulation to reverse established  
168 muscular and peripheral nerve dysfunctions by initiating the treatment at 3 weeks of age,

169 when paralysis was already apparent<sup>19,20</sup> (**Fig. 4a**). We first tested three different doses,  
170 ranging from  $7.5 \times 10^{10}$  to  $3 \times 10^{11}$  viral genome/gram of mouse per AAV9, which was  
171 doubled for the three guide cohorts due to the utilization of two vectors, and found that  
172 the highest dose resulted in homogeneous Lama1-positive fibers (**Fig. S3a**), significant  
173 improvement of muscle function and mobility (**Figs. S3b, S3c**). Longitudinal  
174 measurement of animal mobility and stand-up activity in a non-invasive open field  
175 activity assay showed significant difference between no guide and three guides-treated  
176 mice starting at 5 and 6 weeks old, respectively, which was sustained over time (**Figs.**  
177 **4b, 4c**). Furthermore, specific tetanic force, which measures the aggregate torque  
178 produced by the dorsi flexor muscles, was also improved in the three guides-treated  
179 mice (**Fig. 4d**). In line with this finding, we observed a significant increase in nerve  
180 conduction velocity, which indicates restoration of the myelination defect and contributes  
181 to neuromuscular functionality (**Fig. 4e**). The absence of paralysis in the hind limbs and  
182 markedly improved movement of the mice were evident at the end of the treatment  
183 regimen (**Supplementary videos 3, 4**).

184 Molecular analysis of the treated mice revealed strong Lama1 expression by  
185 immunostaining and western blot (**Figs. 4f, 4g, S4**), which was accompanied by  
186 normalization of  $\alpha$ 4 chain of the laminin subunit (**Figs. S5, S6**)<sup>6</sup>, significant improvement  
187 in muscle histopathology (**Fig. 4h**) and approximately 50% reduction in the fibrotic area  
188 (**Fig. 4i**) compared to the no guide control group. There was a trend towards larger fibers  
189 in the treated mice, although it did not reach statistical significance due to the large  
190 variation between animals (**Fig. 4j**). In addition, upregulation of Lama1 was also  
191 observed in the endoneurium of sciatic nerves and resulted in restoration of myelination  
192 defect (**Figs. 4k, S7**), supporting the improvement of nerve conduction velocity and lack  
193 of paralysis in the mice (**Fig. 4e, Supplementary videos 3, 4**). Quantification of the AAV  
194 genome copy number revealed accumulation of most of the viral genome in the liver,  
195 which is expected from intravenous delivery. Nevertheless, approximately  $1.11 \pm 0.4$  and  
196  $34.1 \pm 4.3$  copies/diploid genome of the viral genome were detected in the sciatic nerves  
197 and skeletal muscles, respectively (**Fig. S8**). Remarkably, even relatively low  
198 transduction efficiency in sciatic nerves was sufficient for functionally significant  
199 upregulation of Lama1 expression.

200 Finally, we investigated the genome wide effects of CRISPR/dCas9-mediated Lama1  
201 upregulation by performing RNA-sequencing on quadriceps muscles isolated from mice  
202 treated with AAV9 carrying no guide and three guides (**Figs. S9, S10, Supplemental**

203 **Tables 1-3).** Age-matched wildtype and  $dy^{2j}/dy^{2j}$  mice served as controls. We observed  
204 a 3.6-log<sub>2</sub>fold upregulation of Lama1 (defined by a false discovery rate, FDR <0.05)  
205 when comparing the mice treated with AAV9 carrying no guide and three guides (**Fig.**  
206 **S9a**). The transcriptional change was even higher at 9-log<sub>2</sub>fold when comparing  
207 untreated  $dy^{2j}/dy^{2j}$  with three guide-treated  $dy^{2j}/dy^{2j}$  (**Fig. S9b, S9c**). Hierarchical  
208 clustering between groups revealed clustering between wildtype and three guides,  
209 whereas the untreated cohort was clustered together with no guide-treated mice (**Figs.**  
210 **S9d, S10**). We also computationally predicted 704 potential off-target binding sites for  
211 the three sgRNAs targeting *Lama1* promoter in the mouse genome, selected based on  
212 the presence of a 6bp PAM-proximal seed sequence and fewer than ten total  
213 mismatches to the cognate target sequence (**Supplemental Tables 4-5**). None of the  
214 top 100 genes contained a predicted off-target site within 60 kilobases of the gene body,  
215 with the average distance from off-target site to the gene body being 2.2 megabases.  
216 Taken together, our results provide strong evidence of the robustness and durability of  
217 CRISPR/dCas9-mediated *Lama1* upregulation for the treatment of MDC1A. Additionally,  
218 we show the therapeutic promise of the strategy for reversal of dystrophic feature in  
219 skeletal muscle and peripheral neuropathy in  $dy^{2j}/dy^{2j}$  mouse model of MDC1A, which  
220 ultimately halts progression of the disease, without any confounding off-target effects.  
221

222 One challenge in developing a therapy for MDC1A is that the heterogeneity of mutations  
223 often leads to variable disease severity and progression. Therefore, there is an urgent  
224 need to develop a universal, mutation-independent strategy that provides a treatment  
225 approach for all patients with MDC1A. Our study establishes a framework in which  
226 CRISPR/dCas9 transcriptional upregulation of a disease modifier gene, such as *Lama1*,  
227 ameliorates disease symptoms *in vivo* and has the potential to be applied to all MDC1A  
228 patients, irrespective of their mutations.

229 Advances have been made towards elucidating MDC1A pathogenesis due to the  
230 availability of several mouse models with absent or reduced *Lama2* expression. Yet, an  
231 important question in the development of therapeutics and clinical trials in MDC1A is the  
232 reversibility of symptoms caused by muscle fibrosis and nerve abnormalities. This issue  
233 has been challenging to address in patients<sup>21</sup>, however, the ability to modify gene  
234 expression in postnatal animals allowed us to address this question and begin to  
235 investigate the therapeutic window of intervention.

236 We have previously demonstrated that an early intervention using CRISPR/Cas9-  
237 mediated correction of a splicing defect resulted in robust *Lama2* restoration and  
238 prevention of disease manifestation <sup>4</sup>. Here we showed that upregulation of *Lama1*,  
239 when initiated at pre-disease-onset, leads to similar prevention. Importantly, when the  
240 therapeutic intervention was initiated at older age, significant rescue of the phenotypes  
241 was attainable, indicating that post-symptomatic treatment provides a significant benefit  
242 in the *dy*<sup>2j</sup>/*dy*<sup>2j</sup> mouse model.

243 In addition to *Lama1* upregulation described in this study, a number of disease modifying  
244 strategies are currently being explored in MDC1A animal models, including treatment  
245 with miniaturized agrin <sup>22-24</sup> and laminin-α1 LN-domain nidogen-1 (αLNND) <sup>25-27</sup>. While  
246 the efficacy of αLNND has only been explored in transgenic mice, AAV-mediated delivery  
247 of mini agrin has been shown to normalize most histopathological parameters in skeletal  
248 muscle, and improve myelination and regeneration of Schwann cells of the peripheral  
249 nerves <sup>22,24</sup>. Despite the observed phenotypic improvement, the mini agrin-treated mice  
250 still have a lower survival rate compared to wild-type animals expressing full-length  
251 agrin, suggesting the potential shortcoming of the shortened version of agrin, which may  
252 be overcome by its full-length form in native glycosylation state <sup>25</sup>. It is important to note  
253 that many preclinical studies in MDC1A were carried out in the more severe *dy*<sup>W</sup>/*dy*<sup>W</sup>  
254 mouse model. Therefore, as a follow up on our study, it will be important to evaluate our  
255 approach in the *dy*<sup>W</sup>/*dy*<sup>W</sup> mice to assess critical parameter such as survival, which is not

256 possible in the  $dy^{2j}/dy^{2j}$  mouse model due to its near-normal life span. Overall, our  
257 approach in combining the CRISPR/dCas9-mediated transcriptional upregulation and  
258 AAV9 as a delivery vehicle can be translated to many other disease modifiers, such as  
259 agrin, as well as conditions where modulation of disease modifiers is required within  
260 both skeletal muscles and peripheral nerves.  
261 In fact, neuromuscular disorders have provided excellent examples to demonstrate the  
262 role of disease modifiers (recently reviewed in<sup>28</sup>). Beyond MDC1A, several studies have  
263 demonstrated that upregulation of *Lama1* stabilizes the sarcolemmal membrane in  
264 dystrophin-deficient mouse models<sup>29</sup>. The most advanced approach is via delivery of  
265 Laminin-111 protein, although the efficacy remains low and the need to produce a large  
266 amount of bioactive protein is challenging<sup>29</sup>. In addition, the utilization of CRISPR/dCas9  
267 system to upregulate *Lama1* in *mdx* mice has been achieved locally via electroporation,  
268 which is not easily translatable into clinical settings<sup>30</sup>. Our strategy of employing AAV-  
269 mediated *S. aureus* dCas9 to upregulate *Lama1* *in vivo* may be tested further as a  
270 potential therapy in the context of Duchenne muscular dystrophy.  
271 In addition, since the CRISPR/dCas9-mediated transcriptional modulation acts directly  
272 on the endogenous locus, it may be used in conjunction with a mutation-correction  
273 approach where the level of restoration of the defective gene is suboptimal, therefore  
274 necessitating further amplification to reach therapeutic efficacy<sup>4,31-36</sup>.  
275 A very recent study by Liao *et al* described utilization of the CRISPR/Cas9 system to  
276 recruit MCP:P65:HSF1 transcriptional activation complex to induce expression of target  
277 genes in skeletal muscle, kidney and liver tissues<sup>18</sup>. This resulted in phenotypic  
278 augmentation such as enhanced muscle mass and substantial improvement in disease  
279 pathophysiology, thereby highlighting the feasibility of using CRISPR/dCas9-mediated  
280 transcriptional activation as a possible therapeutic modality. However, their study relied  
281 almost exclusively on a Cas9-expressing transgenic mouse model or local intramuscular  
282 treatments, and therefore it is difficult to extrapolate the efficacy of this strategy to  
283 disease-relevant models. In contrast, we successfully demonstrated robust upregulation  
284 of *Lama1* after systemic delivery of therapeutic components in a relevant mouse model  
285 of disease that does not constitutively express Cas9.  
286 Finally, the modular nature of the CRISPR/dCas9 system can be utilized to not only to  
287 upregulate, but also to downregulate target gene expression. The latter can be achieved  
288 by coupling dCas9 with transcriptional repressor such as Kruppel-associated box  
289 (KRAB)<sup>17,37</sup>. A very recent study described that following sarcolemmal injury, the muscle

290 membrane resealing process is greatly improved upon the deletion of Osteopontin,  
291 which acts in a concerted fashion with protective modifiers such as Latent TGF- $\beta$  binding  
292 protein (LTBP4) and Annexins 1 and 6<sup>38,39</sup>. The combinatorial effects of such modifiers,  
293 whether they are additive, synergistic or even opposing in action, represent a new  
294 paradigm for lessening disease phenotypes. A foreseeable application of  
295 CRISPR/dCas9-mediated modulation is in the upregulation of protective disease  
296 modifier genes, such as Lama1 or LTBP4, with concurrent downregulation of detrimental  
297 genes, such as Osteopontin, providing a combinatorial therapeutic approach.  
298 In summary, our study establishes a framework to utilize CRISPR/dCas9 to modulate  
299 gene expression of disease modifiers that should be considered as a mutation-  
300 independent therapeutic strategy not only to MDC1A, but also to various other inherited  
301 and acquired diseases.

302 **Methods**

303

304 **Engineering of activation constructs**

305 A fragment containing a catalytically inactive SaCas9 coupled to two flanking VP64  
306 transactivator domains was synthesized by BioBasic Canada and cloned into pX601  
307 (Addgene 61591) using AgeI and EcoRI directional cloning to generate 3XFLAG-VP64-  
308 SadCas9 (D10A/N580A)-NLS-VP64 plasmid (**Figs. 2a, S11, Supplemental Table S6**).  
309 Each sgRNA (**Supplemental Table S6**) was subsequently introduced using Bsal  
310 directional cloning. To generate the three guides only construct (**Fig. 2a**), a fragment  
311 containing three repetitive regions of U6 promoter and *S. aureus* guide scaffold was  
312 assembled, with short linkers in between each region (BioBasic Canada). The fragment  
313 was cloned into KpnI and NotI sites of a pX601-derivative plasmid.

314

315 **Cell Culture**

316 Primary myoblasts were isolated from the Extensor Digitorum Longus (EDL) Muscle of  
317 *dy<sup>2J</sup>/dy<sup>2J</sup>* mice, as previously described<sup>40</sup> and maintained in DMEM supplemented with  
318 1% chicken embryo extract (GeminiBioscience), 10% horse serum, 1%  
319 penicillin/streptomycin and 1% L-glutamine (all from Gibco, unless indicated otherwise).  
320 HEK293 and C2C12 cells where maintained in DMEM supplemented with 10% FBS, 1%  
321 penicillin/streptomycin and 1% L-glutamine (all from Gibco). All cells were maintained at  
322 37°C with 5% CO<sub>2</sub>.

323 Transfection of HEK293T cells was performed as previously described<sup>2</sup>. C2C12 and  
324 *dy<sup>2J</sup>/dy<sup>2J</sup>* cells were transfected in 12-well plates using the Neon Transfection System  
325 (Invitrogen). 400,000 cells were electroporated with 1.5 µg of DNA utilizing optimization  
326 program 16 (pulse voltage: 1400V, pulse width: 20ms, pulse number: 2). Cells were  
327 grown for 72 hours, after which RNA or protein was subsequently collected for protein  
328 analysis and guide screening.

329

330 **Animals, virus production and injections**

331 *dy<sup>2J</sup>/dy<sup>2J</sup>* mice were purchased from the Jackson Laboratory and maintained in the  
332 Toronto Center for Phenogenomics. Both male and female were used in the analyses.  
333 All animal experiments were performed according to Animal Use Protocol number 20-  
334 0305. SadCas9-2xVP64, single guide and three guides plasmids (**Fig. 2a,**  
335 **Supplemental Table S6**) were packaged into AAV9 vectors by Vigene Biosciences as

336 previously described<sup>3</sup>. For intramuscular and temporal vein injection into neonatal pups,  
337 the dose of  $7.5 \times 10^{11}$  viral genomes each was used. Due to the limitation in packaging  
338 capacity, two AAVs were needed for the three guides cohort (**Fig. 2a**), therefore the total  
339 virus injected was  $1.5 \times 10^{12}$  viral genomes per animal. Injection volume was brought to  
340 50  $\mu$ l with 1XPBS (Gibco).

341 For the tail vein injection in young, 3 week old mice, three different doses were initially  
342 tested:  $7.5 \times 10^{10}$ ,  $1.5 \times 10^{11}$  and  $3 \times 10^{11}$  viral genomes per gram of mouse (**Fig. S3**).  
343 Similar to the intramuscular and temporal vein injections, two AAVs were needed for the  
344 three guides cohort, therefore the total dose used in experiments described in **Figs. 4,**  
345 **S4-S10** was  $6 \times 10^{11}$  viral genomes per gram of mouse. Injection volume was brought to  
346 100  $\mu$ l with 1XPBS (Gibco).

347

#### 348 **RNA isolation, guide screening and RT-PCR**

349 RNA was isolated from cultured cells and mouse tissue sections, and cDNA synthesis  
350 was performed as previously described<sup>3</sup>. PCR amplification was utilized to assess the  
351 efficiency of each guide in upregulating *Lama1* expression using a primer in *Lama1* exon  
352 55 (RDC 1919) and a second primer spanning the junction of exons 55 and 56 (RDC  
353 1920). Sequences are listed in **Supplemental Table S6**.  
354 qPCR utilizing Fast SYBR green Master Mix (Qiagen) on a Step One Plus Real Time  
355 PCR (Applied Biosystems) was performed. *Lama1* expression was analyzed using a  
356 primer in *Lama1* exon 55 (RDC 1919) and one spanning the junction of exons 55 and 56  
357 (RDC 1920). Primers against endogenous Gapdh (RDC 345 and 346) were used as an  
358 internal control.  $\Delta\Delta Ct$  was analyzed to assess fold changes between treated and  
359 untreated samples.

360

#### 361 **Protein Isolation and western blot**

362 Protein was isolated from *dy<sup>2j</sup>/dy<sup>2j</sup>* myoblasts and C2C12 cells by adding 150  $\mu$ l of a 1:1  
363 part solution of RIPA homogenizing buffer (50-mM Tris HCl pH 7.4, 150-nM NaCl, 1-mM  
364 EDTA) and RIPA double-detergent buffer (2% deoxycholate, 2% NP40, 2% Triton X-100  
365 in RIPA homogenizing buffer) supplemented with protease-inhibitor cocktail (Roche).  
366 Cells were subsequently scraped from the bottom of each well, collected and incubated  
367 on ice for 30 min. Cells then centrifuged at 12000xg for 15 min at 4°C and the  
368 supernatant was collected and stored at -80°C. Protein from mouse tissue sections was  
369 collected as previously described<sup>3</sup>. Whole protein concentration was measured using

370 Pierce BCA protein assay kit according to the manufacturer's protocol (Thermo Fisher  
371 Scientific). Western blot was performed as previously described<sup>3</sup>. Primary antibodies  
372 used were rabbit Anti-LN $\alpha$ 1 E3 (a gift from Dr. Peter Yurchenco, 0.6  $\mu$ g/ml), mouse  
373 monoclonal M2 anti-Flag (Sigma Aldrich F1804, 1:1000) and rabbit polyclonal anti-  
374 GAPDH (Santa Cruz sc-25778, 1:5000).

375 **Immunofluorescence and H&E staining**

376 Muscles and nerves were sectioned at 8  $\mu$ m thickness and processed for  
377 immunofluorescence analyses according to standard procedures. Antibodies used for  
378 immunofluorescence staining were rat monoclonal against Laminin  $\alpha$ 1 (mAb200,  
379 Durbeej Lab, 1:20),  $\alpha$ 2 (4H8-2, Sigma, 1:500),  $\gamma$ 1 chain (clone A5, Thermo Fisher  
380 Scientific), rabbit polyclonal against Laminin  $\alpha$ 4 chain (kindly provided by Dr. Sasaki),  
381 mouse monoclonal against NF-H (Biolegend SMI 31, 1:1000), goat polyclonal anti-rat  
382 Alexa Fluor 555 (Thermo Fisher Scientific, 1:250) and goat polyclonal anti-mouse Alexa  
383 Fluor 488 (Thermo Fisher Scientific, 1:250). H&E staining was performed as previously  
384 described<sup>4</sup>. Both immunofluorescence and H&E slides were scanned with the 3Dhistech  
385 Pannoramic 250 Flash II digital scanner and analyzed with CaseViewer software, with  
386 the exception of **Figs. S5, S6**, which were analyzed with a Zeiss Axioplan fluorescence  
387 microscope (Carl Zeiss) and images were captured using an ORCA 1394 ER digital  
388 camera (Hamamatsu Photonics) and Open Lab software version 4 (Improvision).

389

390 **Toluidine blue staining and electron microscopy**

391 Freshly isolated mouse sciatic nerves were halved and fixed in a solution of 2%  
392 paraformaldehyde and 2.5% glutaraldehyde in 0.1M sodium cacodylate buffer until  
393 further use. For embedding, the specimens were rinsed with the 0.1M sodium  
394 cacodylate buffer, post-fixed in 1% osmium tetroxide in the washing buffer, dehydrated  
395 in a graded ethanol series followed by propylene oxide, and embedded in Quetol-Spurr  
396 resin overnight at 65°C. Sections of 90nm thickness were cut on a Leica EM UC7  
397 ultramicrotome, stained with uranyl acetate and lead citrate, and imaged on a FEI Tecnai  
398 20 electron microscope at 4400-, 10,000-, and 44,000X magnifications. The same 90nm  
399 sections were stained with toluidine blue and imaged on a Leica DM-2000. All reagents  
400 were purchased from Electron Microscopy Sciences. Quantification of myelin thickness  
401 was measured using ImageJ from at least 14 random axons per field (at least 5 fields  
402 per animal)<sup>41</sup>.

403 **Open field and *in vivo* muscle force assays**

404 Open field activity test and assessment of *in vivo* muscle force were performed on tail  
405 vein injected cohorts at the Lunenfeld-Tanenbaum Research Institute's Centre for  
406 Modeling Human Disease Mouse Phenotyping Facility. For the open field test, mice  
407 were placed in the frontal center of a transparent Plexiglas open field (41.25 cm × 41.25  
408 cm × 31.25 cm) illuminated by 200 lx. A trained operator, who is unaware of the nature  
409 of the projects and treatments, performed experiments. The VersaMax Animal Activity  
410 Monitoring System recorded vertical activities and total distance travelled for 20 minutes  
411 per animal.

412 *In vivo* muscle contraction test was performed using 1300A: 3-in-1 Whole Animal  
413 System and analyzed using Dynamic muscle control/analysis (DMC/DMA) High  
414 throughput software suite (Aurora Scientific). The mice were anaesthetised with  
415 intraperitoneal injection of ketamine/xylazine cocktail at 100 mg/kg and 10 mg/kg of body  
416 weight, respectively. Contractile output was measured via percutaneous electrodes that  
417 stimulate specific nerves innervating the plantar flexors. Specific tetanic force (200 ms of  
418 0.5-ms pulses at 125 Hz) was recorded and corrected to body weight.

419

420 **Nerve conduction velocity**

421 Mice were anesthetized with urethane (1.2 mg/g i.p.) and underwent a tracheotomy to  
422 maintain their airway but were not artificially ventilated. Core body temperature was  
423 maintained at 34-36.5°C using a feedback-controlled heating pad (TR-200; Fine Science  
424 Tools). The sciatic nerve was exposed at two locations via incisions (~15 mm) above the  
425 left knee (site #1) and along the sacral region of the vertebral column (site #2). After  
426 separating the nerve from adjacent tissue, a bipolar hook electrode was applied to the  
427 nerve at each site. Each electrode comprised two chlorided silver wires (0.01" diameter,  
428 A-M systems) placed ~1 mm apart and bent at the tip to form hooks, and attached to a  
429 stimulator (Model DS3, Digitimer Ltd). Stimulating electrodes were insulated from  
430 underlying tissue using a small piece of plastic paraffin film. Stimulus duration was fixed  
431 at 20 µs and current intensity was varied. Stimulus timing was controlled by computer  
432 using a Power1401 computer interface and Signal v5 software (Cambridge Electronic  
433 Design, CED). The compound muscle action potential (CMAP) was recorded using  
434 needle electrodes (~30 G, BD *PrecisionGlide*™), one inserted into the gastrocnemius  
435 muscle and the other (reference) electrode inserted into the Achilles tendon. The CMAP  
436 signal was amplified, low-pass filtered at 10 Hz and high-pass filtered at 1 kHz (DAM 80,

437 World Precision Instruments), and digitized at 40 kHz using the Power1401 and Signal  
438 v5 software (CED). To calculate conduction velocity (CV) from CMAP responses, the  
439 sciatic nerve was stimulated at just-maximal intensity (beyond which there is no change  
440 in CMAP amplitude or latency) three times at site #1 and again three times at site #2.  
441 Nerve conduction velocity was calculated as the difference between average CMAP  
442 latencies for each stimulation site divided by the length of nerve (7.5-10 mm) separating  
443 the sites.

444

#### 445 **Vector genome quantification**

446 Evaluation of AAV genome distribution was performed as previously published<sup>42</sup> with a  
447 few modifications. Genomic DNA was extracted from tibialis anterior, sciatic nerve, and  
448 liver of treated mice using Qiagen Blood and Tissue Kit. 90 ng of DNA was amplified  
449 using primers located in between the two inverted tandem repeats (ITRs) (RDC 1687,  
450 RDC 1679, **Supplemental Table S7**) using Fast SYBR green master mix (Qiagen) on a  
451 Step One Plus Real Time PCR (Applied Biosystems). The Ct value of each reaction was  
452 converted to viral genome copy number by interpolating against the copy number of  
453 standard curve of a known plasmid containing the sgRNA cassette (RDC 362). The  
454 amount of DNA input (90 ng per tissue) was used as a conversion factor to diploid  
455 genome (7 picogram DNA = 1 diploid genome).

456

#### 457 **RNA-Sequencing**

458 Total RNA was isolated from quadriceps muscles using RNeasy kit (Qiagen) and  
459 quantified using Qubit RNA HS assay (Thermo Fisher Scientific). RNA-Sequencing was  
460 performed by the Centre for Applied Genetics in Toronto using the Illumina HiSeq 2500  
461 system, producing 120bp paired-end reads. Raw transcript reads were aligned to the  
462 GRCm38 mouse genome (mm10) using HISAT2<sup>43</sup>. HTSeq was used to determine the  
463 absolute number of read counts for each gene<sup>44</sup>. Only genes with at least 1 read per  
464 million in at least three replicates were kept for downstream analysis. Normalization and  
465 differential expression analysis was completed using the R packages limma, v3.36.3 and  
466 edgeR, v.3.22.3<sup>45</sup>. Differentially expressed genes were defined as genes with a more  
467 than twofold change and adjusted  $P < 0.05$ . Off-target analysis was conducted using a  
468 list of 704 computationally predicted using Cas-OFFinder<sup>46</sup>. Using the Bedtools suite  
469 “closest” function, each of the top 100 differentially expressed genes was matched to the

470 nearest off-target loci to determine the shortest distance from off-target loci to  
471 differentially expressed gene body.

472

### 473 **Statistical Analysis**

474 GraphPad Prism (GraphPad software) was utilized to perform all statistical analyses.  
475 Two-tailed Student' t-tests to evaluate statistical significance between two groups was  
476 performed. Significance was considered to be P < 0.05.

477

### 478 **Data availability**

479 The authors declare that the main data supporting the findings of this study are available  
480 within the article and its Supplementary Information files. Extra data are available from  
481 the corresponding authors upon request.

482

### 483 **Acknowledgements**

484 The Cohn lab members are gratefully acknowledged for the technical support and critical  
485 input in this study. We thank P. Yurchenco (Rutgers University) for providing critical  
486 reagents in this study, C. Rand (Aurora Scientific), I. Vukobradovic (Clinical Phenotyping  
487 Core, Centre for Modeling Human Disease), R. Smith (Prescott Lab) for assistance with  
488 functional and behavioral studies, D. Holmyard (Nanoscale Biomedical Imaging Facility)  
489 for electron microscopy analysis and S. Pereira (The Centre for Applied Genomics) for  
490 genomic data acquisition.

491 This work was supported by AFM-Telethon, Cure CMD, Muscular Dystrophy Association  
492 (to D.U.K), Rare Disease Foundation Microgrant (to P.S.B. and S.E.), SickKids  
493 Restracom (to S.E.), CIHR Summer Studentship (to R.M.), Natural Sciences and  
494 Engineering Research Council of Canada, Canadian Institute for Health Research,  
495 SickKids Foundation and R.S. McLaughlin Foundation Chair in Pediatrics (to R.D.C).

496

### 497 **Author contributions**

498 D.U.K., E.A.I., R.D.C. conceived the study, D.U.K., P.S.B., S.E., D.A.B., K.I.G., K.L.,  
499 E.H., R.K., K.M.P., R.M., performed the experiments, D.A.B., K.I.G., M.D., S.A.P.  
500 provided critical reagents, D.U.K., P.S.B, S.E., D.A.B, K.I.G, S.A.P., E.A.I, R.D.C.  
501 analyzed data, D.U.K, E.A.I., R.D.C. supervised the study, D.U.K. wrote the manuscript  
502 with inputs from the other authors. All authors provided feedback and agreed on the final  
503 manuscript.

504

505  
506

## Figure legends

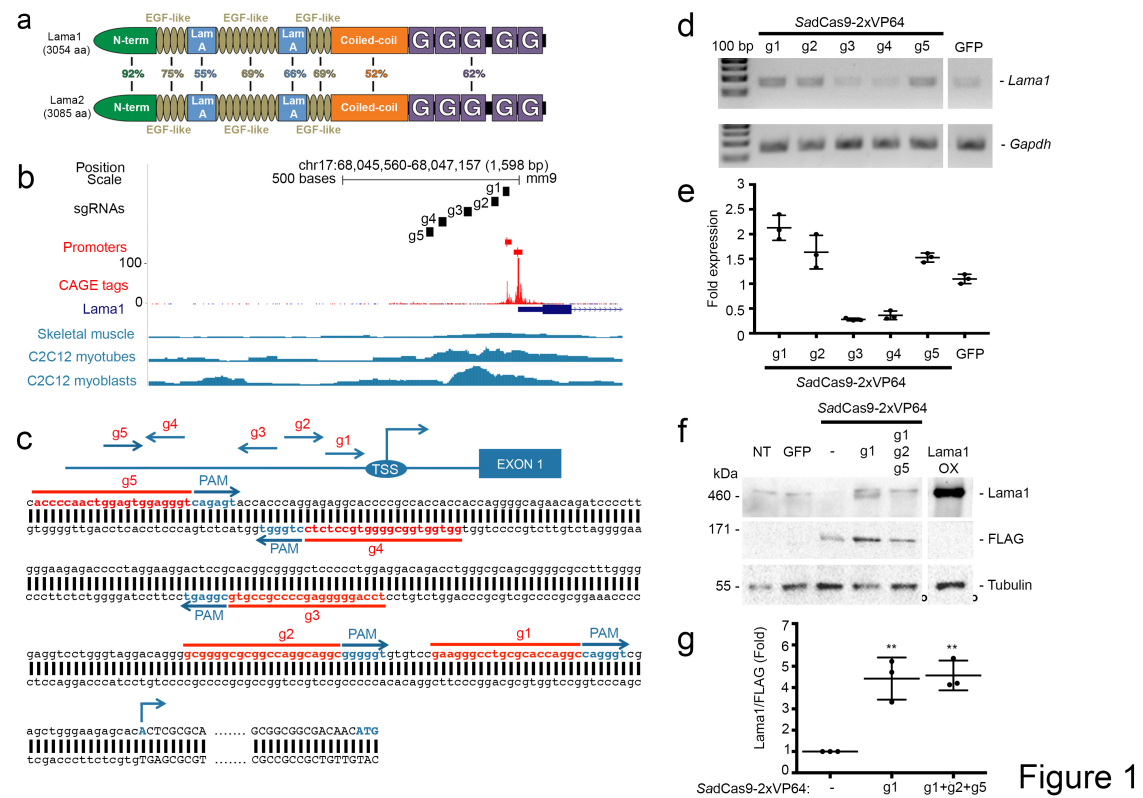


Figure 1

507

508 **Fig. 1. SadCas9-2xVP64-mediated upregulation of *Lama1* in vitro.** (a) *Lama1* and  
509 *Lama2* protein alignment. Total amino acid (aa) and percentage similarity between each  
510 domain are indicated. (b) Analyses of *Lama1* proximal promoter. Five sgRNAs (g1-g5)  
511 were designed in the proximal promoter region of *Lama1* immediately upstream of the  
512 transcription start site (TSS), as indicated by CAGE tags (red). Chromatin accessibility in  
513 skeletal muscle tissue and cells (retrieved using Digital DNase footprinting and ATAC-  
514 Seq) are shown in blue. Data were plotted according to positions from the UCSC  
515 Genome Browser. (c) Positions of the five sgRNAs relative to *Lama1* TSS. Arrowheads  
516 indicate the direction of each sgRNA. Sequences of each sgRNA (red) are immediately  
517 downstream (5') of Sa PAM sequences (NNGRRT) (in blue). ATG indicates translation  
518 start site. (d-e) C2C12 myoblasts were transfected with a plasmid containing SadCas9-  
519 2xVP64 and the corresponding sgRNA(s) targeting *Lama1*, and 72 hours post-  
520 transfection, analyzed by (d) RT-PCR and (e) qRT-PCR. Single and combination of  
521 optimal sgRNAs were transfected into *dy*<sup>2j</sup>/*dy*<sup>2j</sup> myoblasts and *Lama1* protein expression  
522 was assessed by western blot (f). FLAG expression serves as transfection control and  
523 used to (g) normalize *Lama1* upregulation by densitometry analysis. Data are presented

524 as mean  $\pm$  standard deviation from at least three independent experiments. Statistical  
525 analysis was performed using Student's *t*-test. \*\**P*<0.01.

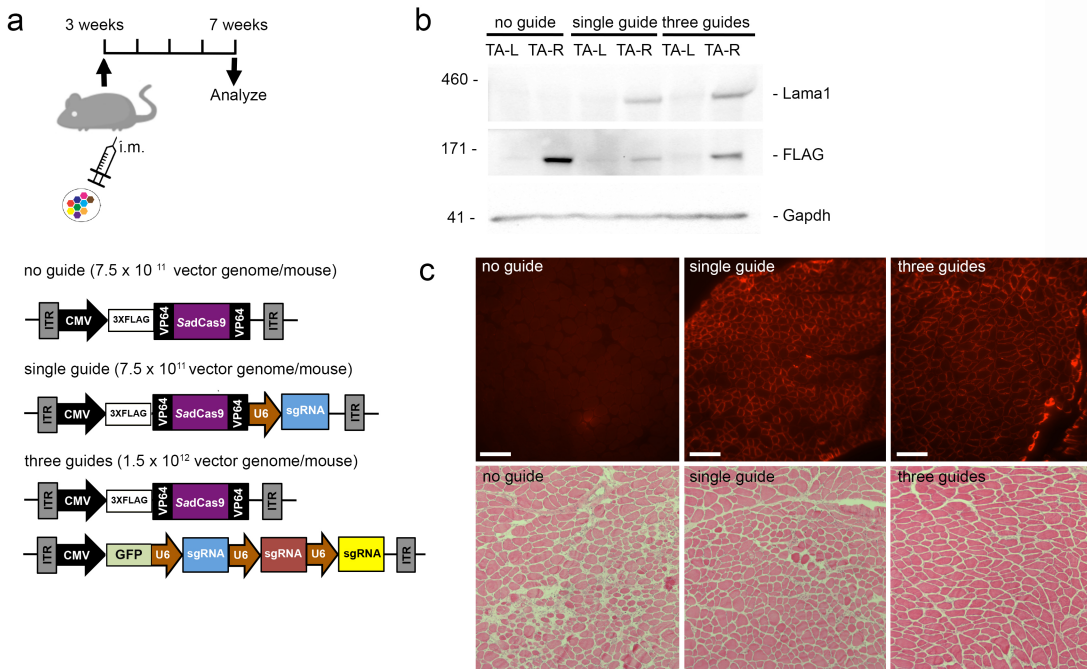


Figure 2

526  
527 **Fig. 2. Upregulation of Lama1 in *tibialis anterior* (TA) muscles of *dy*<sup>2j</sup>/*dy*<sup>2j</sup> mice**  
528 **following intramuscular administration.** (a) Right TA muscles of 3-week old *dy*<sup>2j</sup>/*dy*<sup>2j</sup>  
529 mice were injected with AAV9-carrying no guide (n=4; 7.5x10<sup>11</sup> viral genomes), single  
530 guide (n=4; 7.5x10<sup>11</sup> viral genomes) or three guides (n=4; split into two vectors, thus  
531 total dose was 2x7.5x10<sup>11</sup> viral genomes). ITR: Inverted Terminal Repeats. CMV and U6  
532 promoters are depicted in arrows. Left TA muscles serve as control. (b) Western blot  
533 analysis on Lama1, FLAG-tagged SadCas9, and Gapdh expression. (c)  
534 Immunofluorescence (upper) and H&E (lower) stainings on cross-sections of right TA  
535 muscles from each treatment group. Scale bar: 50  $\mu$ m. Representative images from one  
536 animal per treatment group are shown.

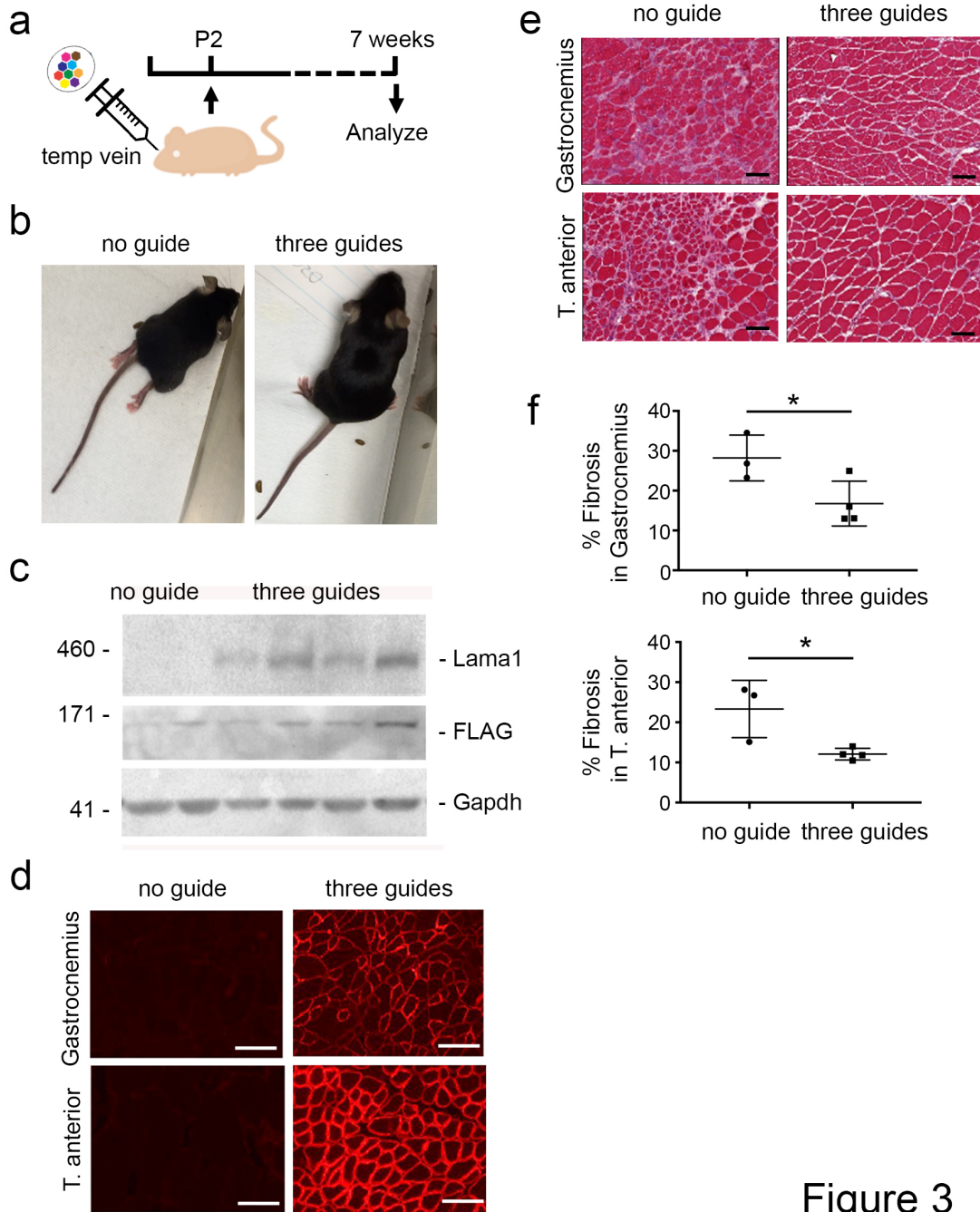


Figure 3

537

538 **Fig. 3. Early intervention to upregulate Lama1 prevents disease progression in**  
539 ***dy<sup>2j</sup>/dy<sup>2j</sup>* mice. (a)** Two-day-old neonatal *dy<sup>2j</sup>/dy<sup>2j</sup>* mice were injected with AAV9 carrying  
540 no guide (n=3; 7.5x10<sup>11</sup> viral genomes) or three guides (n=4; split into two vectors, thus  
541 total dose was 2x7.5x10<sup>11</sup> viral genomes) via temporal vein and sacrificed 7 weeks later.  
542 (b) Photographs of *dy<sup>2j</sup>/dy<sup>2j</sup>* from both treatment groups prior to sacrificing. Note the

543 difference in hindlimb contractures. Lama1 expression was analyzed by (**c**) western blot  
544 and (**d**) immunofluorescence staining, and general histopathology was evaluated by (**e**)  
545 H&E staining. The muscle groups analyzed are indicated on each panel, except on (**c**),  
546 which shows tibialis anterior (TA) muscles. Scale bars: 100  $\mu\text{m}$  (**d**), 200  $\mu\text{m}$  (**e**). (**f**) The  
547 percentage of fibrosis from gastrocnemius (upper) and TA (lower) muscles are  
548 calculated and presented as mean  $\pm$  standard deviation. Statistical analysis was  
549 performed using Student's *t*-test. \* $P<0.05$ .

550

551

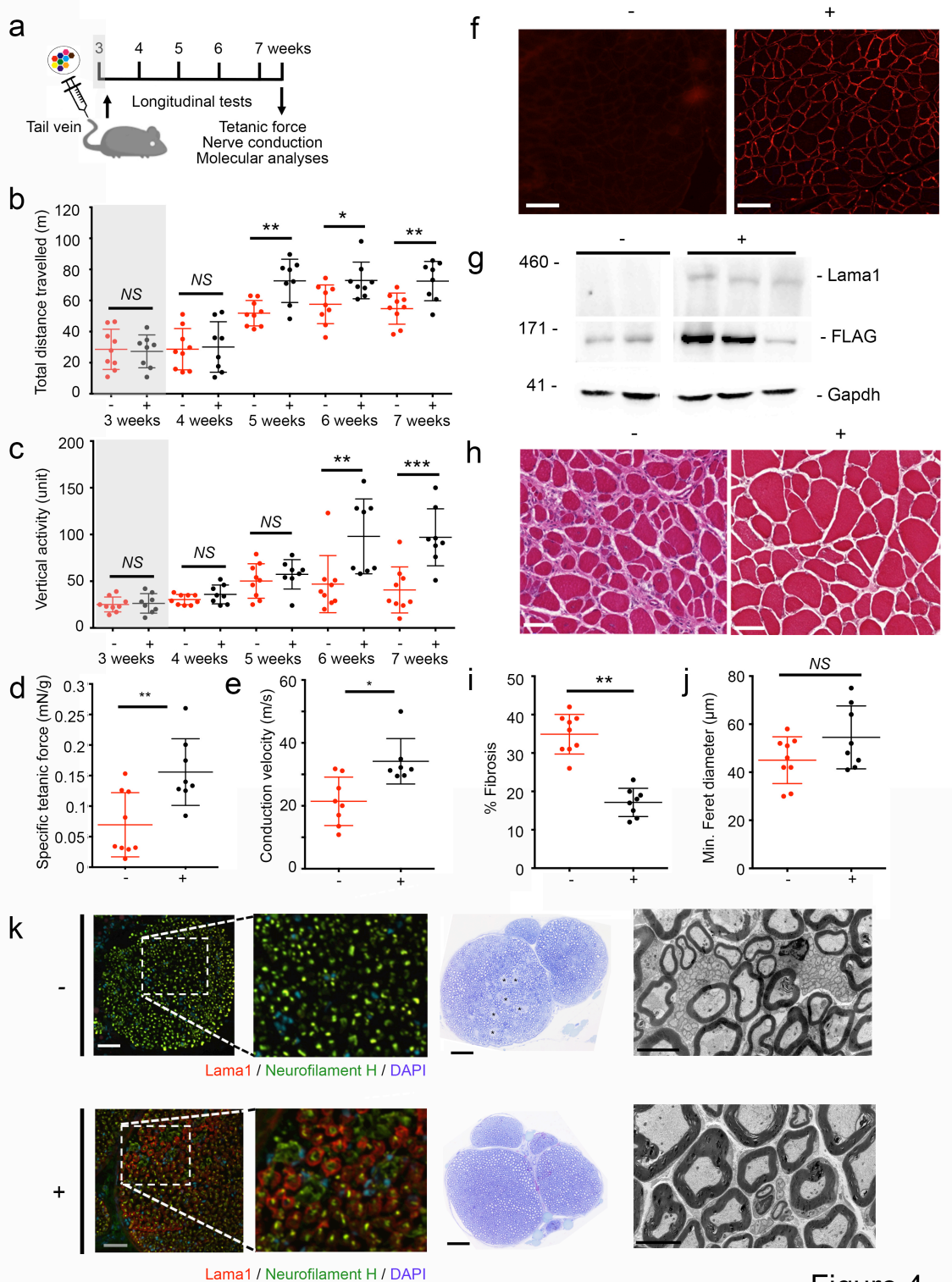


Figure 4

552

553 Fig. 4. Upregulation of *Lama1* in older *dy<sup>2j</sup>/dy<sup>2j</sup>* mice halts disease progression.

554 (a) Three-week old *dy<sup>2j</sup>/dy<sup>2j</sup>* mice were injected with AAV9 carrying no guide (denoted as  
555 -; n=9; 3x10<sup>11</sup> viral genomes/gram) or three guides (denoted as +; n=6; split into two  
556 vectors, thus total dose was 2x3x10<sup>11</sup> viral genomes/gram) via tail vein. Grey box  
557 represents period before treatment. (b, c) Open field activity assay was performed  
558 weekly, before (grey-shaded) and after treatment, and the mice were tested for (d)  
559 muscle contractile and (e) nerve conduction velocity at the end of the treatment regimen,  
560 prior to molecular analyses of the tissues. (f) Immunofluorescence staining and (g)  
561 western blot to analyze Lama1 expression and (h) H&E staining to quantify (i) fibrosis  
562 and (j) fiber size were performed on gastrocnemius muscles. (k) Sciatic nerves were  
563 stained for Lama1 (red) and Neurofilament H (green) (left). Nuclei were counterstained  
564 by DAPI (blue). Higher magnification images from the dotted area are shown.  
565 Representative toluidine blue staining (middle) and electron micrograph (right) are  
566 shown. Asterisks indicate region of myelinated axon fibers. Scale bars: 100 µm (f), 50  
567 µm (h), and 200 µm (k). Data are presented as mean ± standard deviation. Statistical  
568 analysis was performed using Student's *t*-test. \*P<0.05. \*\*P<0.01.

569

570

## 571 References

572

- 573 1. Dowling, J. J., H. D. G., Cohn, R. D., Campbell, C. Treating pediatric neuromuscular  
574 disorders: The future is now. *American journal of medical genetics. Part A* 2017.
- 575 2. Gawlik, K., Miyagoe-Suzuki, Y., Ekblom, P., Takeda, S., Durbeej, M. Laminin alpha1  
576 chain reduces muscular dystrophy in laminin alpha2 chain deficient mice. *Human  
577 molecular genetics* 13:16. 2004.
- 578 3. Yurchenco, P. D., McKee, K. K., Reinhard, J. R., Ruegg, M. A. Laminin-deficient  
579 muscular dystrophy: Molecular pathogenesis and structural repair strategies. *Matrix  
580 biology : journal of the International Society for Matrix Biology* 2017.
- 581 4. Kemaladewi, D. U., Maino, E., Hyatt, E., Hou, H., Ding, M., Place, K. M., Zhu, X.,  
582 Bassi, P., Baghestani, Z., Deshwar, A. G., Merico, D., Xiong, H. Y., Frey, B. J.,  
583 Wilson, M. D., Ivakine, E. A., Cohn, R. D. Correction of a splicing defect in a mouse  
584 model of congenital muscular dystrophy type 1A using a homology-directed-repair-  
585 independent mechanism. *Nat Medicine*. 23:8. 2017.
- 586 5. Sunada, Y., Bernier, S. M., Utani, A., Yamada, Y., Campbell, K. P. Identification of a  
587 novel mutant transcript of laminin alpha 2 chain gene responsible for muscular  
588 dystrophy and dysmyelination in dy2J mice. *Human molecular genetics* 4:6. 1995.
- 589 6. Gawlik, K. I., Harandi, V. M., Cheong, R. Y., Petersen, A., Durbeej, M. Laminin alpha1  
590 reduces muscular dystrophy in dy(2J) mice. *Matrix biology : journal of the  
591 International Society for Matrix Biology* 2018.
- 592 7. Gawlik, K. I., Li, J. Y., Petersen, A., Durbeej, M. Laminin alpha1 chain improves  
593 laminin alpha2 chain deficient peripheral neuropathy. *Human molecular genetics*  
594 15:18. 2006.

- 595 8. Gawlik, K. I., Mayer, U., Blomberg, K., Sonnenberg, A., Ekblom, P., Durbeej, M.  
596 Laminin alpha1 chain mediated reduction of laminin alpha2 chain deficient muscular  
597 dystrophy involves integrin alpha7beta1 and dystroglycan. *FEBS letters* 580:7. 2006.  
598 9. Gawlik, K. I., Akerlund, M., Carmignac, V., Elamaa, H., Durbeej, M. Distinct roles for  
599 laminin globular domains in laminin alpha1 chain mediated rescue of murine laminin  
600 alpha2 chain deficiency. *PloS one* 5:7. 2010.  
601 10. Gawlik, K. I., Durbeej, M. Transgenic overexpression of laminin alpha1 chain in  
602 laminin alpha2 chain-deficient mice rescues the disease throughout the lifespan.  
603 *Muscle & nerve* 42:1. 2010.  
604 11. Maeder, M. L., Linder, S. J., Cascio, V. M., Fu, Y., Ho, Q. H., Joung, J. K. CRISPR  
605 RNA-guided activation of endogenous human genes. *Nature methods* 10:10. 2013.  
606 12. Perez-Pinera, P., Kocak, D. D., Vockley, C. M., Adler, A. F., Kabadi, A. M., Polstein,  
607 L. R., Thakore, P. I., Glass, K. A., Ousterout, D. G., Leong, K. W., Guilak, F.,  
608 Crawford, G. E., Reddy, T. E., Gersbach, C. A. RNA-guided gene activation by  
609 CRISPR-Cas9-based transcription factors. *Nature methods* 10:10. 2013.  
610 13. Gonzalez, S., Fernando, R. N., Perrin-Tricaud, C., Tricaud, N. In vivo introduction of  
611 transgenes into mouse sciatic nerve cells in situ using viral vectors. *Nature protocols*  
612 9:5. 2014.  
613 14. Wojtal, D., Kemaladewi, D. U., Malam, Z., Abdullah, S., Wong, T. W., Hyatt, E.,  
614 Baghestani, Z., Pereira, S., Stavropoulos, J., Mouly, V., Mamchaoui, K., Muntoni, F.,  
615 Voit, T., Gonorazky, H. D., Dowling, J. J., Wilson, M. D., Mendoza-Londono, R.,  
616 Ivakine, E. A., Cohn, R. D. Spell Checking Nature: Versatility of CRISPR/Cas9 for  
617 Developing Treatments for Inherited Disorders. *Am J Hum Genet* 98:1. 2016.  
618 15. Ran, F. A., Cong, L., Yan, W. X., Scott, D. A., Gootenberg, J. S., Kriz, A. J., Zetsche,  
619 B., Shalem, O., Wu, X., Makarova, K. S., Koonin, E. V., Sharp, P. A., Zhang, F. In  
620 vivo genome editing using *Staphylococcus aureus* Cas9. *Nature* 520:7546. 2015.  
621 16. Esvelt, K. M., Mali, P., Braff, J. L., Moosburner, M., Yaung, S. J., Church, G. M.  
622 Orthogonal Cas9 proteins for RNA-guided gene regulation and editing. *Nature  
623 methods* 10:11. 2013.  
624 17. Qi, L. S., Larson, M. H., Gilbert, L. A., Doudna, J. A., Weissman, J. S., Arkin, A. P.,  
625 Lim, W. A. Repurposing CRISPR as an RNA-guided platform for sequence-specific  
626 control of gene expression. *Cell* 152:5. 2013.  
627 18. Liao, H. K., Hatanaka, F., Araoka, T., Reddy, P., Wu, M. Z., Sui, Y., Yamauchi, T.,  
628 Sakurai, M., O'Keefe, D. D., Nunez-Delicado, E., Guillen, P., Campistol, J. M., Wu, C.  
629 J., Lu, L. F., Esteban, C. R., Izpisua Belmonte, J. C. In Vivo Target Gene Activation  
630 via CRISPR/Cas9-Mediated Trans-epigenetic Modulation. *Cell* 171:7. 2017.  
631 19. Pasteuning-Vuhman, S., Putker, K., Tanganyika-de Winter, C. L., Boertje-van der  
632 Meulen, J. W., van Vliet, L., Overzier, M., Plomp, J. J., Aartsma-Rus, A., van Putten,  
633 M. Natural disease history of the dy2J mouse model of laminin alpha2 (merosin)-  
634 deficient congenital muscular dystrophy. *PloS one* 13:5. 2018.  
635 20. Kemaladewi, D. U., Benjamin, J., Hyatt, E., Ivakine, E. A., Cohn, R. D. Increased  
636 polyamine as protective disease modifier in Congenital Muscular Dystrophy. *Human  
637 molecular genetics* 2018.  
638 21. Bonnemann, C. G., Wang, C. H., Quijano-Roy, S., Deconinck, N., Bertini, E.,  
639 Ferreiro, A., Muntoni, F., Sewry, C., Beroud, C., Mathews, K. D., Moore, S. A., Bellini,  
640 J., Rutkowski, A., North, K. N., Members of International Standard of Care Committee  
641 for Congenital Muscular, D. Diagnostic approach to the congenital muscular  
642 dystrophies. *Neuromuscular disorders : NMD* 24:4. 2014.  
643 22. Qiao, C., Li, J., Zhu, T., Draviam, R., Watkins, S., Ye, X., Chen, C., Li, J., Xiao, X.  
644 Amelioration of laminin-alpha2-deficient congenital muscular dystrophy by somatic

- 645 gene transfer of miniagrin. *Proceedings of the National Academy of Sciences of the*  
646 *United States of America* 102:34. 2005.
- 647 23. Bentzinger, C. F., Barzaghi, P., Lin, S., Ruegg, M. A. Overexpression of mini-agrin in  
648 skeletal muscle increases muscle integrity and regenerative capacity in laminin-  
649 alpha2-deficient mice. *FASEB journal : official publication of the Federation of*  
650 *American Societies for Experimental Biology* 19:8. 2005.
- 651 24. Qiao, C., Dai, Y., Nikolova, V. D., Jin, Q., Li, J., Xiao, B., Li, J., Moy, S. S., Xiao, X.  
652 Amelioration of Muscle and Nerve Pathology in LAMA2 Muscular Dystrophy by AAV9-  
653 Mini-Agrin. *Molecular Therapy* 9:2018.
- 654 25. Meinen, S., Barzaghi, P., Lin, S., Lochmuller, H., Ruegg, M. A. Linker molecules  
655 between laminins and dystroglycan ameliorate laminin-alpha2-deficient muscular  
656 dystrophy at all disease stages. *The Journal of cell biology* 176:7. 2007.
- 657 26. Reinhard, J. R., Lin, S., McKee, K. K., Meinen, S., Crosson, S. C., Sury, M., Hobbs,  
658 S., Maier, G., Yurchenco, P. D., Ruegg, M. A. Linker proteins restore basement  
659 membrane and correct LAMA2-related muscular dystrophy in mice. *Science*  
660 *translational medicine* 9:396. 2017.
- 661 27. McKee, K. K., Crosson, S. C., Meinen, S., Reinhard, J. R., Ruegg, M. A., Yurchenco,  
662 P. D. Chimeric protein repair of laminin polymerization ameliorates muscular  
663 dystrophy phenotype. *The Journal of clinical investigation* 127:3. 2017.
- 664 28. Hightower, R. M., Alexander, M. S. Genetic modifiers of Duchenne and  
665 facioscapulohumeral muscular dystrophies. *Muscle & nerve* 57:1. 2018.
- 666 29. Rooney, J. E., Gurpur, P. B., Burkin, D. J. Laminin-111 protein therapy prevents  
667 muscle disease in the mdx mouse model for Duchenne muscular dystrophy.  
668 *Proceedings of the National Academy of Sciences of the United States of America*  
669 106:19. 2009.
- 670 30. Perrin, A., Rousseau, J., Tremblay, J. P. Increased Expression of Laminin Subunit  
671 Alpha 1 Chain by dCas9-VP160. *Molecular therapy. Nucleic acids* 6:2017.
- 672 31. Yuan, J., Ma, Y., Huang, T., Chen, Y., Peng, Y., Li, B., Li, J., Zhang, Y., Song, B.,  
673 Sun, X., Ding, Q., Song, Y., Chang, X. Genetic Modulation of RNA Splicing with a  
674 CRISPR-Guided Cytidine Deaminase. *Molecular cell* 72:2. 2018.
- 675 32. Villiger, L., Grisch-Chan, H. M., Lindsay, H., Ringnalda, F., Pogliano, C. B., Allegri,  
676 G., Fingerhut, R., Haberle, J., Matos, J., Robinson, M. D., Thony, B., Schwank, G.  
677 Treatment of a metabolic liver disease by in vivo genome base editing in adult mice.  
678 *Nature medicine* 24:10. 2018.
- 679 33. Bengtsson, N. E., Hall, J. K., Odom, G. L., Phelps, M. P., Andrus, C. R., Hawkins, R.  
680 D., Hauschka, S. D., Chamberlain, J. R., Chamberlain, J. S. Muscle-specific  
681 CRISPR/Cas9 dystrophin gene editing ameliorates pathophysiology in a mouse  
682 model for Duchenne muscular dystrophy. *Nature communications* 8:2017.
- 683 34. Nelson, C. E., Hakim, C. H., Ousterout, D. G., Thakore, P. I., Moreb, E. A., Rivera,  
684 R. M., Madhavan, S., Pan, X., Ran, F. A., Yan, W. X., Asokan, A., Zhang, F., Duan,  
685 D., Gersbach, C. A. In vivo genome editing improves muscle function in a mouse  
686 model of Duchenne muscular dystrophy. *Science* 2015.
- 687 35. Tabebordbar, M., Zhu, K., Cheng, J. K., Chew, W. L., Widrick, J. J., Yan, W. X.,  
688 Maesner, C., Wu, E. Y., Xiao, R., Ran, F. A., Cong, L., Zhang, F., Vandenberghe, L.  
689 H., Church, G. M., Wagers, A. J. In vivo gene editing in dystrophic mouse muscle and  
690 muscle stem cells. *Science* 2015.
- 691 36. Long, C., Amoasii, L., Mireault, A. A., McAnally, J. R., Li, H., Sanchez-Ortiz, E.,  
692 Bhattacharyya, S., Shelton, J. M., Bassel-Duby, R., Olson, E. N. Postnatal genome  
693 editing partially restores dystrophin expression in a mouse model of muscular  
694 dystrophy. *Science* 2015.

- 695 37. Thakore, P. I., D'Ippolito, A. M., Song, L., Safi, A., Shivakumar, N. K., Kabadi, A. M.,  
696 Reddy, T. E., Crawford, G. E., Gersbach, C. A. Highly specific epigenome editing by  
697 CRISPR-Cas9 repressors for silencing of distal regulatory elements. *Nature methods*  
698 12:12. 2015.
- 699 38. Lamar, K. M., Bogdanovich, S., Gardner, B. B., Gao, Q. Q., Miller, T., Earley, J. U.,  
700 Hadhazy, M., Vo, A. H., Wren, L., Molkentin, J. D., McNally, E. M. Overexpression of  
701 Latent TGFbeta Binding Protein 4 in Muscle Ameliorates Muscular Dystrophy through  
702 Myostatin and TGFbeta. *PLoS genetics* 12:5. 2016.
- 703 39. Quattrocelli, M., Capote, J., Ohiri, J. C., Warner, J. L., Vo, A. H., Earley, J. U.,  
704 Hadhazy, M., Demonbreun, A. R., Spencer, M. J., McNally, E. M. Genetic modifiers of  
705 muscular dystrophy act on sarcolemmal resealing and recovery from injury. *PLoS*  
706 *genetics* 13:10. 2017.
- 707 40. Kemaladewi, D. U., de Gorter, D. J., Aartsma-Rus, A., van Ommen, G. J., ten Dijke, P., t Hoen, P. A., Hoogaars, W. M. Cell-type specific regulation of myostatin signaling.  
708 *FASEB journal : official publication of the Federation of American Societies for  
709 Experimental Biology* 26:4. 2012.
- 710 41. Zhang, Y., Argaw, A. T., Gurfein, B. T., Zameer, A., Snyder, B. J., Ge, C., Lu, Q. R.,  
711 Rowitch, D. H., Raine, C. S., Brosnan, C. F., John, G. R. Notch1 signaling plays a  
712 role in regulating precursor differentiation during CNS remyelination. *Proceedings of  
713 the National Academy of Sciences of the United States of America* 106:45. 2009.
- 714 42. Hakim, C. H., Wasala, N. B., Pan, X., Kodippili, K., Yue, Y., Zhang, K., Yao, G.,  
715 Haffner, B., Duan, S. X., Ramos, J., Schneider, J. S., Yang, N. N., Chamberlain, J. S.,  
716 Duan, D. A Five-Repeat Micro-Dystrophin Gene Ameliorated Dystrophic Phenotype in  
717 the Severe DBA/2J-mdx Model of Duchenne Muscular Dystrophy. *Molecular therapy.  
718 Methods & clinical development* 6:2017.
- 719 43. Kim, D., Langmead, B., Salzberg, S. L. HISAT: a fast spliced aligner with low  
720 memory requirements. *Nature methods* 12:4. 2015.
- 721 44. Anders, S., Pyl, P. T., Huber, W. HTSeq--a Python framework to work with high-  
722 throughput sequencing data. *Bioinformatics* 31:2. 2015.
- 723 45. Ritchie, M. E., Phipson, B., Wu, D., Hu, Y., Law, C. W., Shi, W., Smyth, G. K. limma  
724 powers differential expression analyses for RNA-sequencing and microarray studies.  
725 *Nucleic acids research* 43:7. 2015.
- 726 46. Bae, S., Park, J., Kim, J. S. Cas-OFFinder: a fast and versatile algorithm that  
727 searches for potential off-target sites of Cas9 RNA-guided endonucleases.  
728 *Bioinformatics* 30:10. 2014.
- 729  
730  
731

**Extended data/supplementary figures**

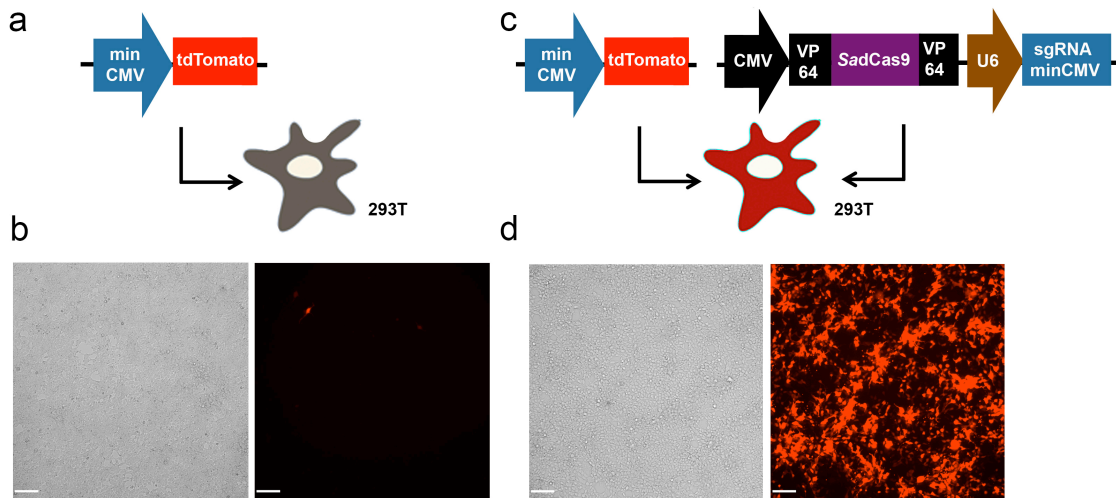


Figure S1

**Fig. S1. SadCas9-2xVP64 enhances expression of minCMV-driven *tdTomato* *in vitro*.** HEK293T was transfected with (a,b) a plasmid containing minCMV-driven *tdTomato* gene only, or (c,d) in combination with a plasmid containing SadCas9-2xVP64 and a sgRNA targeting the minCMV promoter. (b,d) Cells were imaged for *tdTomato* expression by fluorescent microscopy. Scale bar: 50  $\mu$ m.

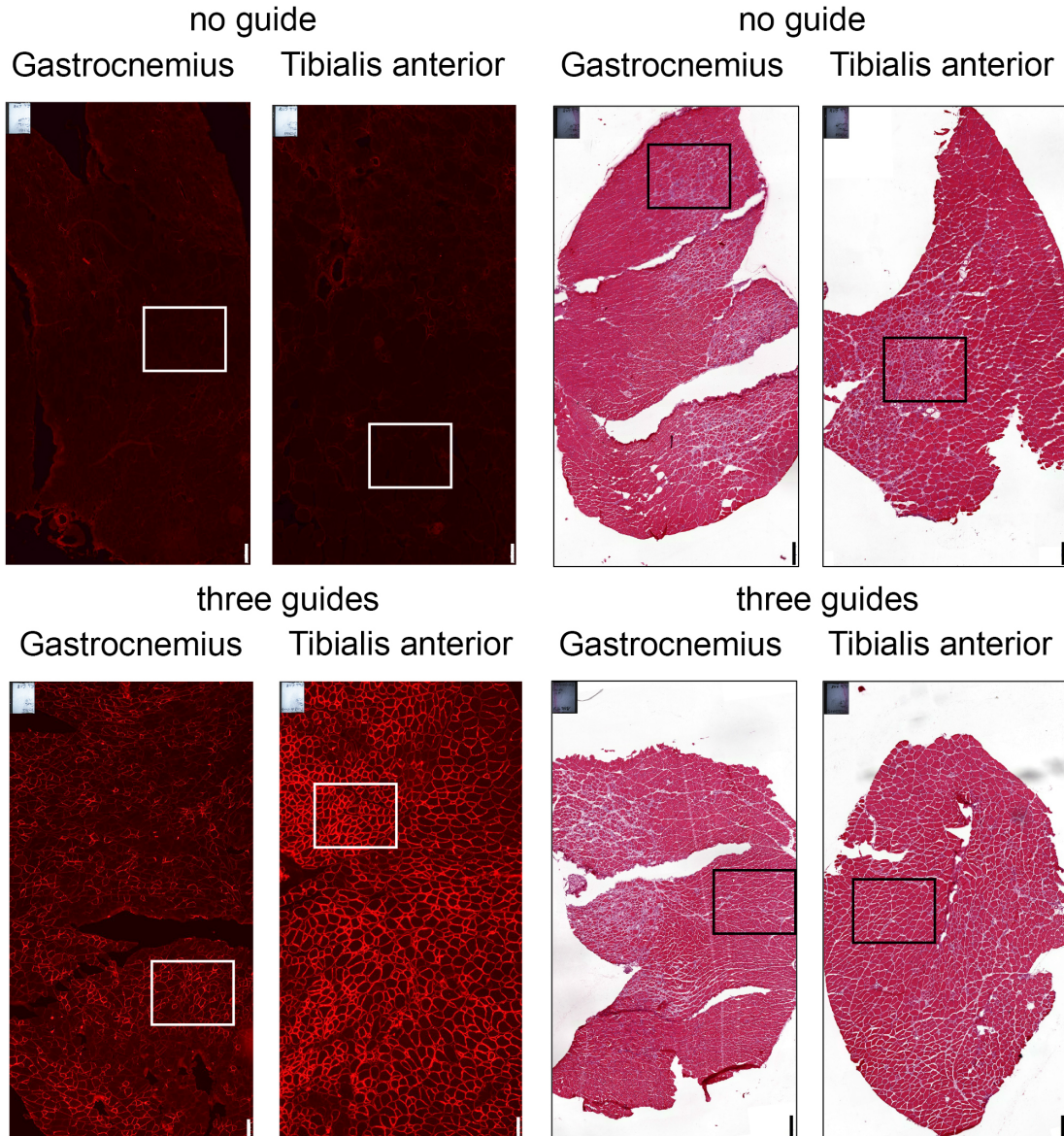


Figure S2

**Fig. S2. Expression of Lama1 and muscle architecture following early intervention in neonatal  $dy^{2j}/dy^{2j}$  mice.** Lower magnification of immunofluorescence and H&E staining images of Fig. 3 in the main manuscript.

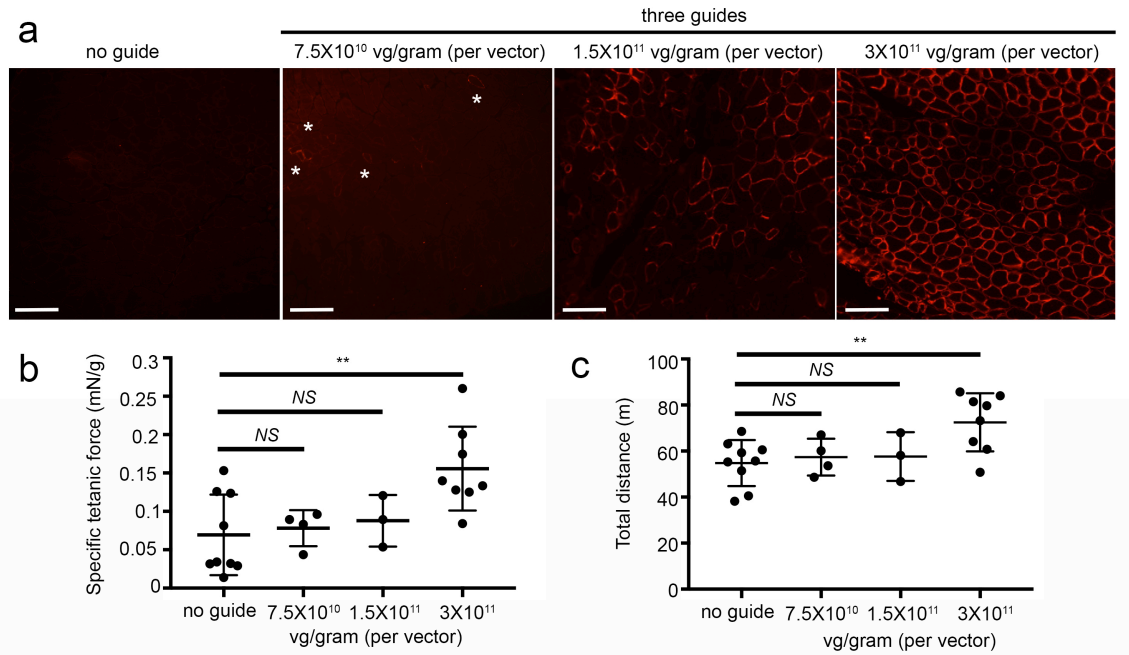


Figure S3

**Fig. S3. Upregulation of Lama1 corresponds to improvement of muscle functions.**

Three-weeks old *dy<sup>2j</sup>/dy<sup>2j</sup>* mice were injected systemically via tail vein with different doses of AAV9: 7.5x10<sup>10</sup>, 1.5x10<sup>11</sup>, or 3x10<sup>11</sup> viral genome (vg)/gram of mouse. Two AAVs were necessary for the three guide cohort, therefore the total doses of virus injected was 1.5x10<sup>11</sup>, 3x10<sup>11</sup>, and 6x10<sup>11</sup> viral genomes/gram of mouse. TA muscles isolated four weeks later were stained for Lama1 expression (a). Asterisks indicate Lama1-positive fibers in the low dose cohort. Scale bar: 100 μm. *In vivo* contractile force assay (b) and open field test (c) performed in the end of the treatment regimen. Data are presented as average ± standard deviation. Statistical analysis was performed using one-way ANOVA. NS: not significant. \*\*P<0.01.

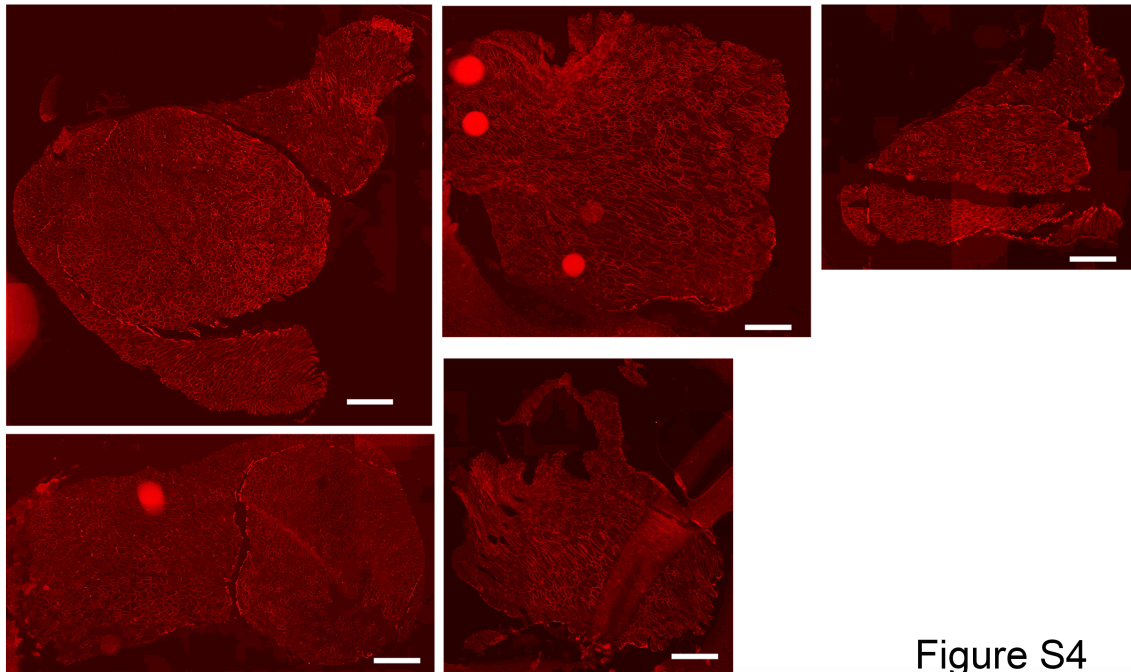


Figure S4

**Fig. S4. Representative images of *Lama1*-positive muscle sections**

Mice were injected systemically with three guides at the age of three weeks old via tail vein, and sacrificed at the age of 11-12 weeks old. Muscles were stained for *Lama1* expression (red). Scale bar: 500  $\mu$ m.

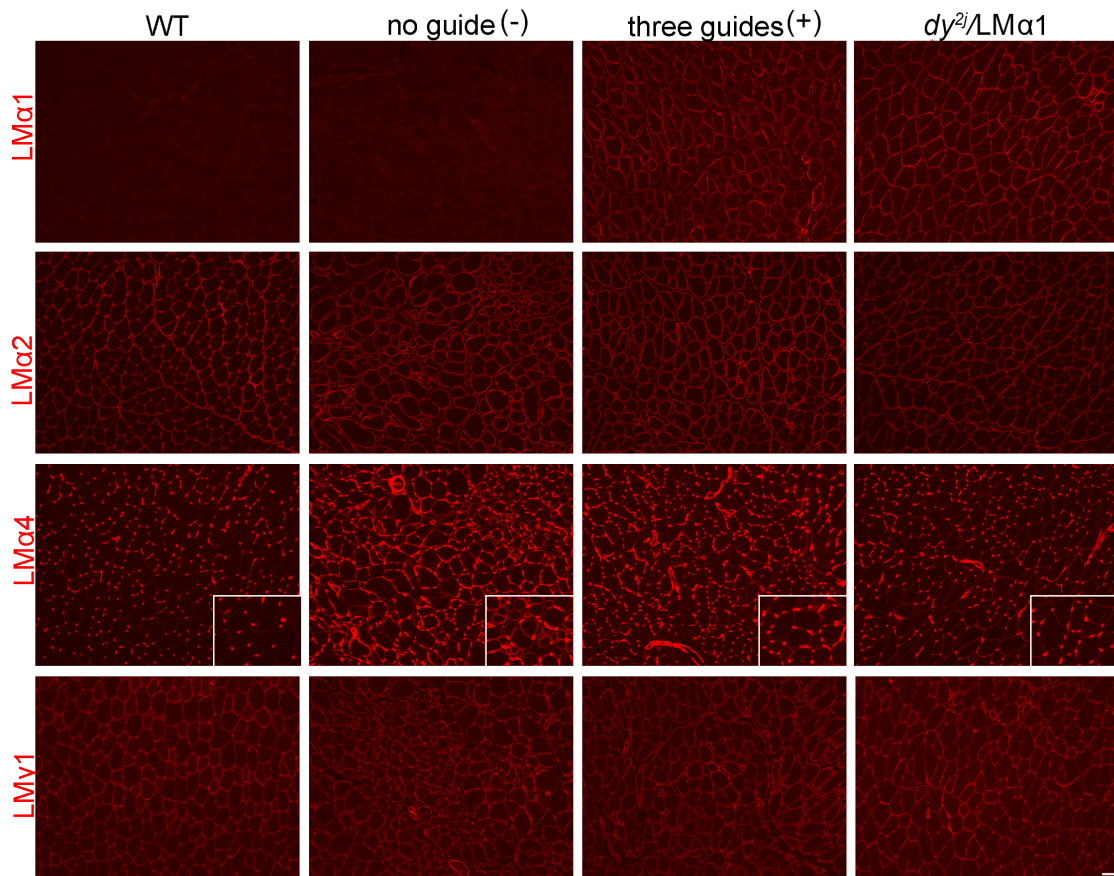


Figure S5

**Fig. S5. Expression of Laminin (LM) subunits in tibialis anterior muscles.**

Expression of LM subunits in tibialis anterior from wild-type,  $dy^{2j}/dy^{2j}$  (intravenously injected with AAV carrying no guide or three guides) and  $dy^{2j}/LM\alpha 1$  (with transgenic overexpression of  $LM\alpha 1$ ) mice (n=3 for each group). Expression of  $LM\alpha 1$  chain in tibialis anterior is comparable between  $dy^{2j}/dy^{2j}$  AAV-three guide-treated mice and transgenic mice. No major differences in expression of  $LM\alpha 2$  and  $LMy1$  were detected between the groups.  $LM\alpha 4$  chain is upregulated in muscle from  $dy^{2j}/dy^{2j}$  AAV-no guide-treated mice and its expression is partially normalized in muscle from  $dy^{2j}/dy^{2j}$  AAV-three guide treated mice. Scale bar: 50 $\mu$ m.

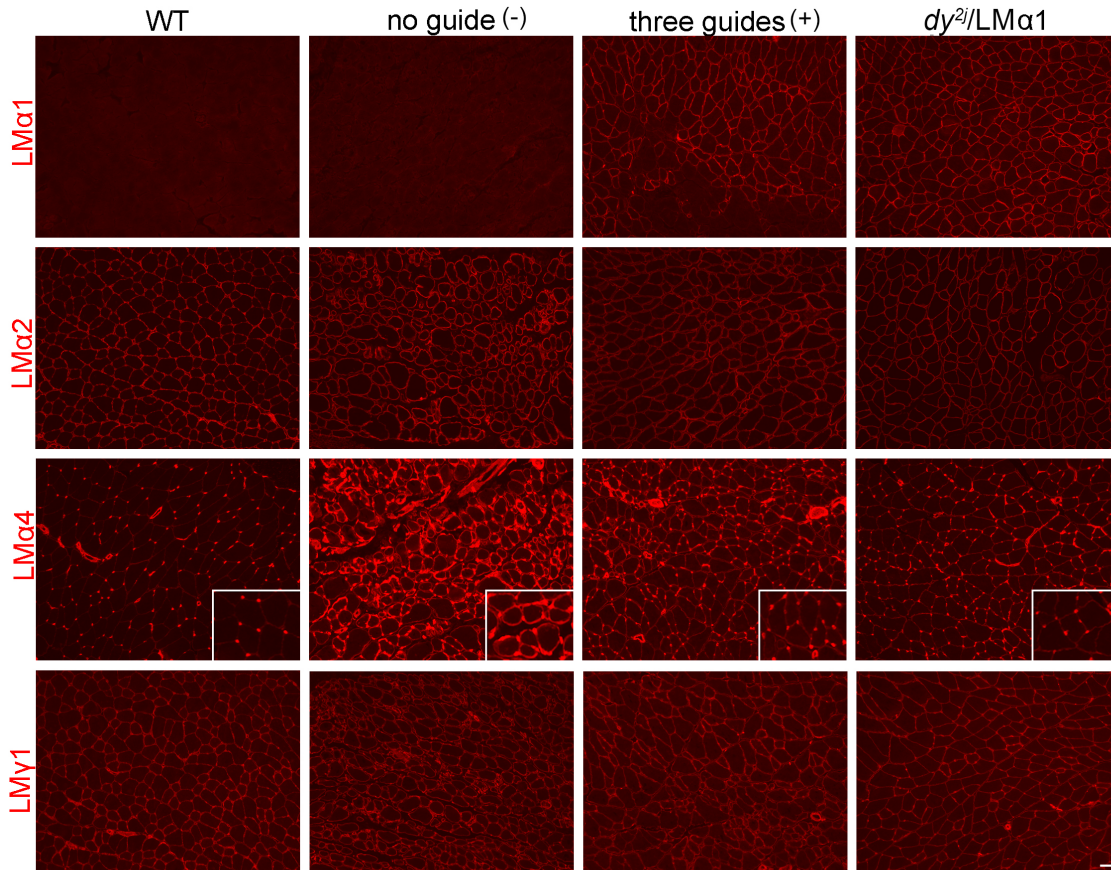


Figure S6

**Fig. S6. Expression of Laminin (LM) subunits in gastrocnemius muscles.**

Expression of LM subunits in tibialis anterior from wild-type,  $dy^{2j}/dy^{2j}$  (intravenously injected with AAV carrying no guide or three guides) and  $dy^{2j}/LM\alpha 1$  (with transgenic overexpression of  $LM\alpha 1$ ) mice (n=3 for each group). Expression of  $LM\alpha 1$  chain in tibialis anterior is comparable between  $dy^{2j}/dy^{2j}$  AAV-three guide-treated mice and transgenic mice. No major differences in expression of  $LM\alpha 2$  and  $LMy1$  were detected between the groups.  $LM\alpha 4$  chain is upregulated in muscle from  $dy^{2j}/dy^{2j}$  AAV-no guide-treated mice and its expression is partially normalized in muscle from  $dy^{2j}/dy^{2j}$  AAV-three guide treated mice. Scale bar: 50 $\mu$ m.

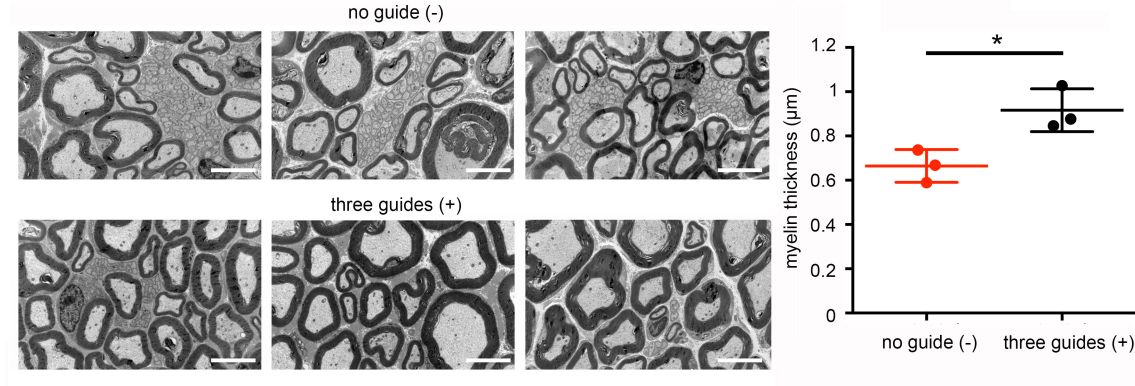


Figure S7

**Fig. S7. Myelination of sciatic nerves.**

Electron microscopy images of sciatic nerves isolated from  $dy^{2j}/dy^{2j}$  mice injected with AAV carrying no guide or three guides ( $n=3$  for each group). Myelin thickness was quantified using ImageJ and presented as average  $\pm$  standard deviation. Statistical analysis was performed using Student's *t*-test. \* $P<0.05$ . Scale bar: 5  $\mu\text{m}$ .

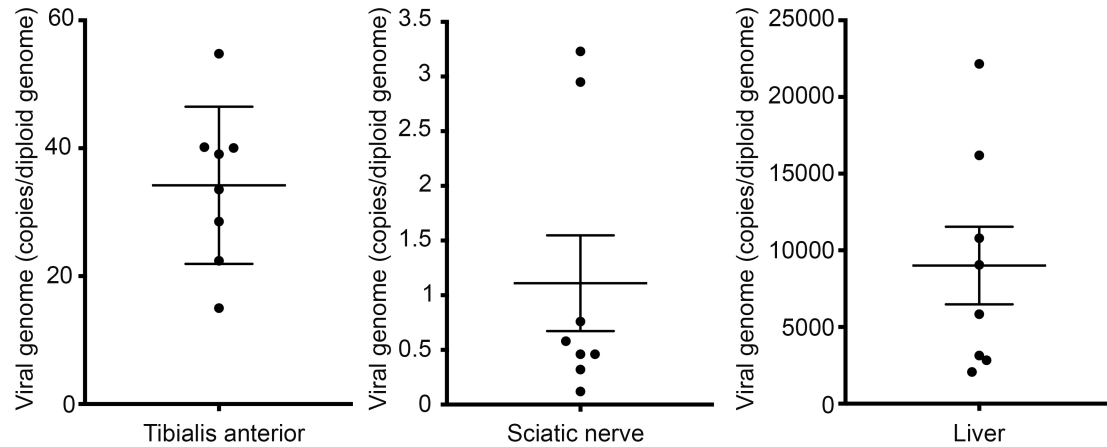


Figure S8

**Fig. S8. Quantitative evaluation of AAV genome distribution.**

Genomic DNA isolated from tibialis anterior muscle, sciatic nerve and liver of dy2j mice injected with AAV carrying three guides ( $n=8$ ) was amplified for the presence of viral genome by qPCR. Data are presented as average  $\pm$  SEM.

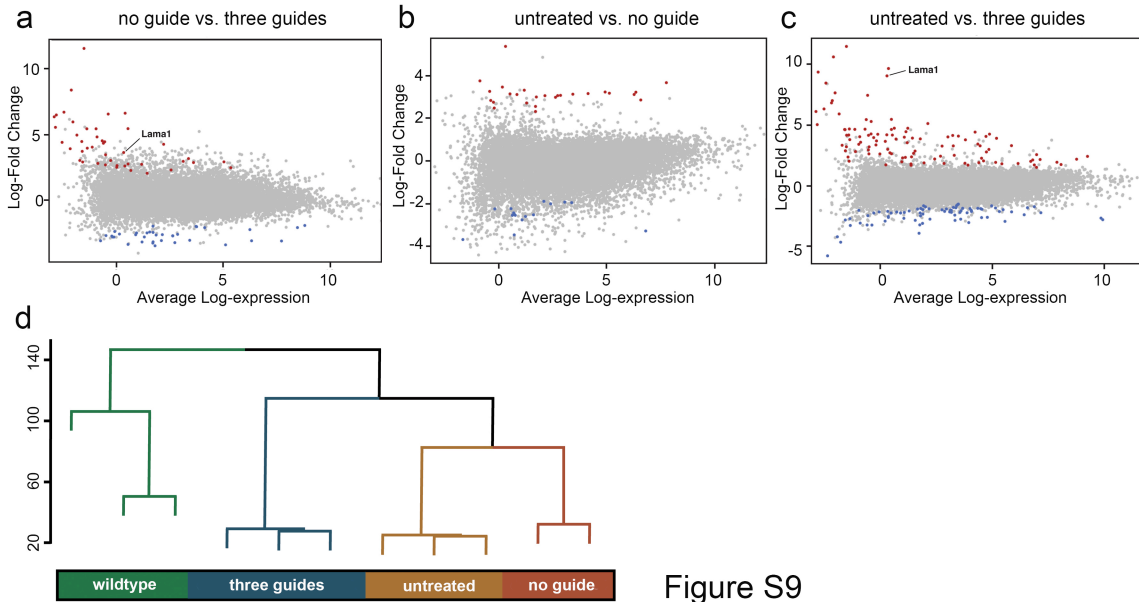


Figure S9

**Fig. S9. Genome-wide analysis of gene expression of SadCas9-VP64-treated *dy*<sup>2j</sup>/*dy*<sup>2j</sup> mice.**

Differential expression analysis derived from RNA-Sequencing results from the quadriceps of treated and untreated mice (**a-c**), comparing SadCas9-2xVP64 alone and SadCas9-2xVP64 with three guides targeting Lama1 (**a**), untreated to SadCas9-2xVP64 alone (**b**), and untreated to SadCas9-2xVP64 with three guides targeting Lama1 (**c**). Gene significantly differentially expressed, (FDR < 0.05), are coloured. Red data points indicate a log-fold change greater than one, while blue data points indicate a log-fold change less than one. Hierarchical clustering was performed on the normalized counts-per-million expression data (**d**).

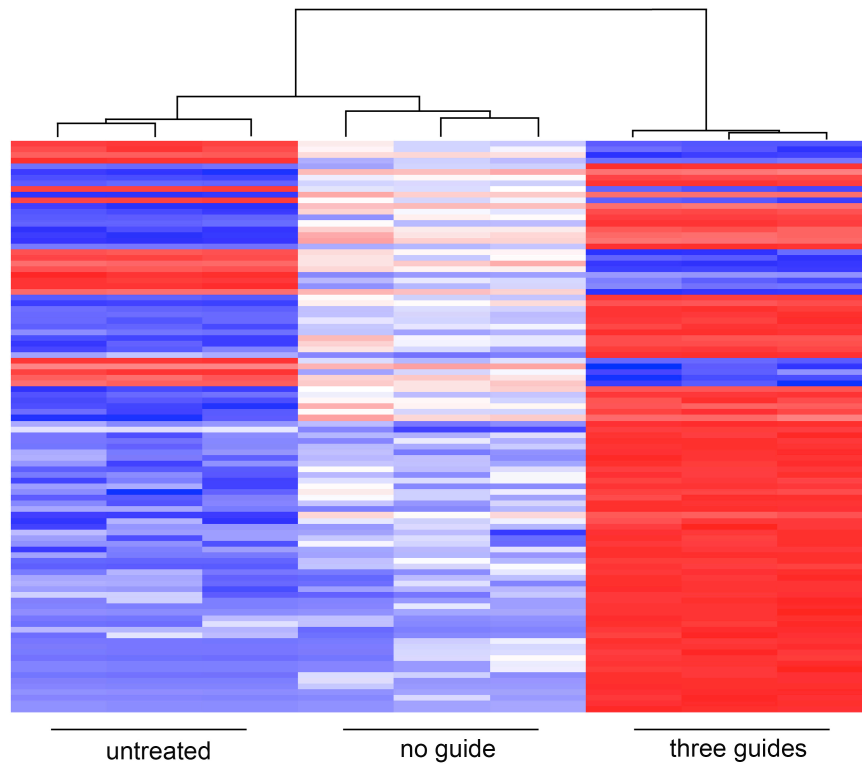


Figure S10

**Fig. S10. Top 100 differentially expressed genes.**

Heatmap illustrating normalized log-CPM values for the top 100 genes differentially expressed in SadCas9-2xVP64 with three guide treated quadriceps versus untreated quadriceps. Red indicates higher expression while blue indicates lower expression.

Start            3X FLAG  
**M - DYKDHDG DYKDHDIDYKDDDK** - HGPRA -  
                  VP64  
DALDDFDLDMGLGSDALDDFDLDMGLGSDALDDFDLDMGLGSDALDDFDLDM -  
                  NLS  
VN - **PKKKRKV** - GIHGVPA -  
                  D10A  
**KRNYILGLA\*IGITSGVGIIIDYETRDVIDAGVRLFKEANVENNEGRRSKRGARRL**  
**KRRRRRHRIQRVKKLLFDYNLLTDHSELSGINPYEARVKGLSQKLSEEEFSAALLHLAK**  
**RRGVHNVNEVEEDTGNELSTKEQISRNSKALEEKYVAELQLERLKKDGEVRGSINRF**  
**KTSDYVKEAKQLLKVKAYHQLDQSFIPTYIDLLETTRRTYYEGPGEGSPFGWKDIKE**  
**WYEMLMGHCTYFPEELRSVKYAYNADLYNALNDLNNLVITRDENEKLEYYEKFQIEN**  
**VFKQKKKPTLKQIAKEILVNEEDIKGYRVTSTGKPEFTNLKVYHDIKDITARKEIIENAEI**  
**LDQIAKILTIYQSSEDIQEELTNLNELTQEEEIQISNLKGYTGTHNLSLKAINLILDELWH**  
**TNDNQIAIFNRLKLPKKVDLSQQKEIPTTLVDDFILSPVVKRSFIQSIVNAIIKKYGLP**  
**N580A**  
**GKCLYSLEAPILEDLLNNPFNYEVDHIIIPRSVSFDNSFNNKVLVKQEEA\*SKGNRTPF**  
**QYLSSSDSKISYETFKKHILNLAKGKG RISKTKKEYLLEERDINRFSVQKDFINRNLVDT**  
**RYATRGLMNLLRSYFRVNNLDVKVKSINGGFTSFLRRKWFKKERNKGYKHHAEDA**  
**LIIANADFIFKEWKKLDKAKKVMENQMFEEKQAESMPEIETEQEYKEIFITPHQIKHIKD**  
**FKDYKYSHRVDKKPNNRELINDTLYSTRKDDKGNTLIVNNLNGLYDKDNDKLKKLINKS**  
**PEKLLMYHHDPQTYQKLKLIMEQYGDEKNPLYKYYEETGNYLTKYSKKDNGPVIKKIK**  
**YYGNKLNAHLDITDDYPNSRNKVVKLSLKPYRFDVYLDNGVYKFVTVKNLDVIKKENY**  
**YEVNSKCYEEAKKLKISNQAEFIASFYNNDLIKINGELYRIGVNNNDLLNRIEVNMIDIT**  
**YREYLENMNDKRPPRIIKTIASKTQSICKYSTDILGNLYEVKSKKHPQIICKKG -**  
                  NLS  
**KRPAATKKAGQAKKKK** - GS -  
                  VP64  
DALDDFDLDMGLGSDALDDFDLDMGLGSDALDDFDLDMGLGSDAL DDFDLDM

**Fig. S11. Protein encoded in the SadCas9-VP64 transcriptional activator plasmid.**

Different domains are annotated accordingly. Amino acids encoding SadCas9 are in bold and italic, and the mutated residues D10A and N580A are indicated in red asterisk (\*). NLS: Nuclear localization signal.

### **Supplemental video legends**

#### **Video S1. Phenotype of control $dy^{2j}/dy^{2j}$ mouse following early intervention.**

The  $dy^{2j}/dy^{2j}$  mouse was injected with AAV9 containing SadCas9-2xVP64 (no guide) at P2 (pre-symptomatic stage) via temporal vein and video was taken at the age of 7-week old. Hind limb paralysis, contracture and kyphosis resulting from lack of functional *Lama2* and compensatory *Lama1* are apparent.

#### **Video S2. Phenotype of treated $dy^{2j}/dy^{2j}$ mouse following early intervention.**

The  $dy^{2j}/dy^{2j}$  mouse was injected with AAV9 containing SadCas9-2xVP64 and sgRNAs targeting *Lama1* proximal promoter (three guides) at P2 (pre-symptomatic stage) via temporal vein and video was taken at the age of 7-week old. Upregulation of compensatory *Lama1* expression ameliorates the hind limb paralysis, contracture and kyphosis.

#### **Video S3. Phenotype of control $dy^{2j}/dy^{2j}$ mouse following intervention at symptomatic stage.**

The  $dy^{2j}/dy^{2j}$  mouse was injected with AAV9 containing SadCas9-2xVP64 (no guide) at 3-week old (pre-symptomatic stage) via tail vein. Video was taken at the age of 7-week old. Hind limb paralysis, contracture and kyphosis resulting from lack of functional *Lama2* and compensatory *Lama1* are apparent.

#### **Video S4. Phenotype of treated $dy^{2j}/dy^{2j}$ mouse following intervention at symptomatic stage.**

The  $dy^{2j}/dy^{2j}$  mouse was injected with AAV9 containing SadCas9-2xVP64 and sgRNAs targeting *Lama1* proximal promoter (three guides) at 3-week old (pre-symptomatic stage) via tail vein. Video was taken at the age of 7-week old. Dystrophic features and disease progression were significantly improved and partially reversed following upregulation of *Lama1*.

## **Supplemental tables**

**Supplemental table 1.** Top 100 genes differentially expressed in “SadCas9-2xVP64 + three guides” compared to “untreated”

**Supplemental table 2.** Top 100 genes differentially expressed in “SadCas9-2xVP64 + three guides” compared to “SadCas9-2xVP64 + no guide”

**Supplemental table 3.** Top 100 genes differentially expressed in “SadCas9-2xVP64 + no guide” compared to “untreated”

**Supplemental table 4.** Analysis showing distance from off-target site to differentially expressed gene body

**Supplemental table 5.** List of computationally predicted off-target sites

**Supplemental table 6.** Primers, plasmids and sgRNAs used in this study



















**Supplemental Table 6. Primers, plasmids and sgRNAs used in this study**

	Name	Sequences (5' to 3')	ID Number
Primers	U6_gRNA_PCR_F	GAG GGC CTA TTT CCC ATG ATT CCT	RDC 255
	dTomato_guide_B	AAA CCA CTG TGG GGT GGA GGG GAC	RDC 1194
	mGAPDH F	TGTTTGTGATGGGTGTGAACC	RDC 345
	mGAPDH R	ACTGTGGTCATGAGCCCTTC	RDC 346
	Lama1 Primer FW	GGAAAGGTTACAAAGTCGATTGG	RDC 977
	Lama1 Primer RV	ACGTGAAATAAGACCTGCCATC	RDC 978
	Lama1 qPCR 1 KL F	TTTCTTGAAAGGAAGCGGATATG	RDC 1918
	Lama1 qPCR 2 KL F	TGGGTCCATTAACAGAAGGAAAG	RDC 1919
	Lama1 qPCR 2 KL R	ATGGGTGAAGTCCAAAAGTTGAG	RDC 1920
	Vector genome F	ATGGTGAGCAAGGGCGAGG	RDC 1687
	Vector genome R	AGCTTGCCGTAGGTGGCATC	RDC 1679

	Name	ID number
Plasmids	minCMV-tdTomato	RDC 262
	px601 SadCas9-VP64	RDC 153
	3-guide cassettes	RDC 367

	Name	Sequences (5' to 3')	PAM
sgRNAs	<i>tdTomato</i> sgRNA Top	CACCGTCCCCTCCACCCCACAGTG	AAGAAT
	<i>tdTomato</i> sgRNA Bottom	AAACCACTGTGGGTGGAGGGGAC	
	<i>Lama1</i> sgRNA1 Top	CACCGAAGGGCCTGCGCACCGAGC	CAGGGT
	<i>Lama1</i> sgRNA1 Bottom	AAACGCCTGGTGCAGGCCCTTC	
	<i>Lama1</i> sgRNA2 Top	CACCGCGGGGCAGGCCAGGCAGGC	GGGGGT
	<i>Lama1</i> sgRNA2 Bottom	AAACGCCTGCCTGGCCGCAGCCCCGC	
	<i>Lama1</i> sgRNA3 Top	CACCGTCCAGGGGAGCCCCGCCGTG	CGGAGT
	<i>Lama1</i> sgRNA3 Bottom	AAACCACGGCGGGCTCCCCCTGGAC	
	<i>Lama1</i> sgRNA4 Top	CACCGGTGGTGGCGGGGTGCCTCTC	CTGGGT
	<i>Lama1</i> sgRNA4 Bottom	AAACGAGAGGCACCCGCCACCAACC	
	<i>Lama1</i> sgRNA5 Top	CACCGACCCCAACTGGAGTGGAGGGT	CAGAGT
	<i>Lama1</i> sgRNA5 Bottom	AAACACCCCTCCACTCCAGTTGGGGTC	